Anti-PD-1 immunotherapy leads to tuberculosis reactivation via dysregulation of TNF-α

Liku B Tezera[1,2], Magdalena K Bielecka[1], Paul Ogongo[3,4], Naomi F Walker[5,6,7], Matthew Ellis[8], Diana J Garay-Baquero[1,2], Kristian Thomas[1], Michaela Reichmann[1], Dave A Johnston[1], Katalin A Wilkinson[9], Mohamed Ahmed[3], Sanjay Jogai[1], Suwan Jayasinghe[10], Robert J Wilkinson[9,11], Salah Mansour[1,2], Gareth Thomas[8], Christian Ottensmeier[8], Alasdair Leslie[3,12], Paul Elkington[1,2]

[1]NIHR Biomedical Research Centre, School of Clinical and Experimental Sciences, Faculty of Medicine, University of Southampton, UK. [2]Institute for Life Sciences, University of Southampton, UK. [3]Africa Health Research Institute, KwaZulu Natal, South Africa. [4]Department of Tropical and Infectious Diseases, Institute of Primate Research, National Museums of Kenya, Nairobi, Kenya. [5]Wellcome Centre for Infectious Diseases Research in Africa, Institute of Infectious Disease and Molecular Medicine, University of Cape Town, South Africa. [6]TB Centre and Department of Clinical Research, London School of Hygiene and Tropical Medicine, London, UK. [7]Department of Clinical Sciences, Liverpool School of Tropical Medicine, Liverpool, UK. [8]School of Cancer Sciences, University of Southampton, UK. [9] The Francis Crick Institute, London, UK. [10]BioPhysics Group Department of Mechanical Engineering, University College London, UK. [11]Department of Infectious Diseases, Imperial College London, UK. [12]Department of Infection and Immunity, University College London, UK.

26   **Address for correspondence:**

27   Dr Liku B Tezera

28   Clinical and Experimental Sciences

29   University of Southampton, Southampton SO16 1YD

30   Tel.:   00 44 23 8079 6671

31   E-mail: l.tezera@soton.ac.uk

32

33   **Running title:** PD-1 inhibition and TB reactivation

34

35

36   **Abstract**

37

38   Previously, we developed a 3-dimensional cell culture model of human tuberculosis (TB) and

39   demonstrated its potential to interrogate the host-pathogen interaction (Tezera et al, 2017).

40   Here, we use the model to investigate mechanisms whereby immune checkpoint therapy for

41   cancer paradoxically activates TB infection. In patients, PD-1 is expressed in *Mycobacterium*

42   *tuberculosis* (Mtb)-infected lung tissue but absent in areas of immunopathology. In the

43   microsphere model, PD-1 ligands are up-regulated by infection, and the PD-1/PD-L1 axis is

44   further induced by hypoxia. Inhibition of PD-1 signalling increases Mtb growth, and

45   augments cytokine secretion. TNF-α is responsible for accelerated Mtb growth, and TNF-α

46   neutralisation reverses augmented Mtb growth caused by anti-PD-1 treatment. In human TB,

47   pulmonary TNF-α immunoreactivity is increased and circulating PD-1 expression negatively

48   correlates with sputum TNF-α concentrations. Together, our findings demonstrate that PD-1

49   regulates the immune response in TB, and inhibition of PD-1 accelerates Mtb growth via

50   excessive TNF-α secretion.

51

Introduction

Tuberculosis (TB) continues to be a global health pandemic, killing more people than any other infection (1). TB involves a complex host-pathogen interaction, with humans and *Mycobacterium tuberculosis* (Mtb) having undergone prolonged co-evolution (2). TB has often been thought to primarily result from loss of immune control, because approximately 90% individuals infected with TB never progress to active disease, and this progression is increased in the context of immune deficiency; such as in cases of HIV infection, in infants, people with genetic deficiency of the IL-12/IFN-γ signalling pathway or after anti-TNF-α antibody treatment (3). However, an emerging concept is that an excessive immune response to Mtb may be equally harmful. Standard disease paradigms predict that immune activation resulting from the administration of checkpoint inhibitors should lead to better control of Mtb infection (4). However, counter-intuitively these agents seem to be activating TB, as evidenced by recent reports of TB developing in patients treated for malignancy with immune checkpoint inhibition, often rapidly after commencing therapy (5-15). Consistent with this emerging clinical phenomenon, programmed death (PD-1) deficient mice are highly susceptible to TB, dying more rapidly than T-cell deficient mice (16, 17).

PD-1 and its ligand PD-L1 are expressed in human granulomas (10), suggesting a regulatory role at the site of disease. TB granulomas are hypoxic (18), and PD-L1 is up-regulated by hypoxia (19), further suggesting a mechanistic link between hypoxia and the PD-1/PD-L1 axis within TB lesions. In this study, we investigate the expression patterns of PD-1 and PDL-1 within TB infected human lung tissue and the relationship between PD-1 and anti-TB immunity. Next, using a human 3D cell culture model of TB (20), we show that hypoxia increases expression of PD-1 and its ligands, that PD-1 inhibition increases Mtb growth.

4

77   Surprisingly, TNF-α is primarily responsible for this effect, and TNF-α neutralisation

78   reverses the anti-PD-1 induced phenotype.

79

80   **Results**

81

82   **PD-1 is expressed in human TB granulomas but not in areas of immunopathology**

83   First, we investigated the presence and localisation of PD-1-expressing T cells in human

84   pulmonary TB. We hypothesised that PD-1 would be expressed by T cells in the lung of

85   patients with TB, and at a higher frequency than in the blood. In thirty-five patients

86   undergoing medically indicated lung resection to treat TB or TB sequalae, PD-1 expression

87   was measured on T cells isolated from the lung and matched blood samples, available for 23

88   patients, by flow cytometry. Overall, PD-1 expression in homogenized lung tissue was highly

89   variable, with a trend towards increased PD-1 in both CD4 and CD8 T-cells from the lung

90   compared to matched blood, which reached statistical significance for CD8 T-cells (Figure

91   1A). Lung tissue from healthy individuals was not available for study, however, the median

92   frequency of 11 and 14% of PD-1 +ve CD4 and CD8 T-cells observed are generally lower

93   than recently reported for healthy human lung tissue from organ donors of approximately

94   50% for both cell types (21). As lung tissue is highly perfused with blood, distinguishing

95   cells of lung or blood origin is challenging.

96

97   To explore this further, we stained lung samples for canonical markers of tissue resident T-

98   cells, CD69 and CD103 (21). PD-1 expression on lung CD4 cells was predominantly

99   restricted CD69+ve T-cells, with a smaller proportion also expressing CD103 (Fig.1B,

100   overall frequencies Supplemental file 1), consistent with a tissue resident phenotype and in

101   contrast to PD-1 expressing cells in blood, which are largely CD69 negative (Figure 1–figure

102   supplement 1). Lung CD8 T-cells were also found to predominantly express CD69 in

103   addition to CD103, again in contrast to CD8 T-cells in circulation. Therefore, these data are

104   consistent with expression of PD-1 on lung tissue resident T-cells in patients with active or

105   previous pulmonary TB infection. However, TB immunopathology is highly heterogenous

106   within the lung and these analyses do not provide information as to the localization of PD-1

107   expression within TB lesions.

108

109   To address this question, we performed immunohistochemical analysis of human lung

110   biopsies of patients with active TB. Within stable granulomas with an intact cellular

111   structure, PD-1 expression was present around the central macrophage core (Figure 1C-i).

112   Both CD4 and CD8 T cells were present in the granuloma (Figure 1C-ii and -iii), and co-

113   localisation analysis demonstrated that a proportion of both T cell subtypes expressed PD-1

114   (Figure 1C-iv), consistent with the flow cytometry data. In contrast, in caseating granulomas

115   with evident immunopathology, PD-1 expression was totally absent (Figure 1D-i and Figure

116   1–figure supplement 2). The lack of immunoreactivity was not due to lack of viable cells, as

117   CD4 and CD8 expressing T cells were present within the same area (Figure 1D-ii and -iii).

118   Therefore, in human granulomas, PD-1 is expressed in areas where the host-pathogen

119   interaction appears stable but is absent in regions of immunopathology.

120

121   **The PD-1/ PD-L1 axis is up-regulated in the 3D microsphere model**

122   Taken together, these data from Mtb infected patients demonstrate that PD-1 is expressed by

123   lung resident T-cells and may be required to prevent destructive lung disease. However,

124   whether this is a causal associated remains unclear. We therefore explored the biological role

125   of PD-1 expression in a 3-dimensional (3D) human tissue culture model. TB is a human

126   disease characterised by a prolonged host-pathogen interaction in 3D, and is regulated by the

127   extracellular matrix, and previously we have previously developed a 3D cell culture model

128   incorporating extracellular matrix to investigate TB pathogenesis (20, 22). Here, we first

129   studied migration of cells within the alginate-collagen matrix by performing time-lapse

130   microscopy (Figure 2A and Video 1). For this experiment only, UV killed Mtb was used to

131   permit the imaging outside the containment level 3 laboratory. From 24h, progressive

132   accumulation occurs around a central infected core, resulting in a large multicellular

133   granuloma by 48h with dynamic cellular movement similar to the T cell mobility observed in

134   mouse BCG granulomas (23).

135

136   We next investigated whether the PD-1/PD-L1 axis was up-regulated by infection in this 3D

137   model, and found that Mtb infection increased PD-L1 and PD-L2 gene expression at 4 days

138   post infection (Figure 2B). Furthermore, a hypoxic environment (1% oxygen) further

139   increased PD-L2 expression. PD-1 gene expression was not increased at 72h by Mtb infection

140   under normoxic conditions, but was up-regulated when infected cells were incubated in

141   hypoxia (Figure 2B). The change in expression required both infection and hypoxia, as

142   hypoxia did not increase PD-1 or PD-L1/2 expression alone (Figure 2–figure supplement 1).

143   We then studied PD-1/PD-L1 cellular surface expression in microspheres by flow cytometry

144   after one week of infection. Mtb infection slightly increased PD-1 surface expression on

145    $CD4^+$ T cells in normoxia, which was augmented by hypoxia (Figure 2C). Similarly, Mtb

146   infection increased PD-1 expression on $CD8^+$ T cells, which was greater in hypoxia (Figure

147   2D). Furthermore, on $CD14^+CD11b^+$ cells, PD-L1 expression was increased by infection and

148   more so in hypoxia (Figure 2E). To investigate whether the effect of hypoxia on increased

149   PD-1/PD-L1 expression was due to altered Mtb growth, we studied proliferation using Mtb

150   expressing firefly luciferase and also colony counting on Middlebrook 7H11 agar. Hypoxia

151   inhibited Mtb growth by both readouts (Figure 2F and Figure 2–figure supplement 2A). As

152   expected, hypoxia also increased expression of the hypoxia inducible factor, HIF-1α, in host

153   cells (Figure 2G), but did not have a significant effect on host cell survival (Figure 2–figure

154   supplement 2B). Therefore, the increased PD-1 and PD-L1/2 expression in hypoxia was not

155   due to increased Mtb growth or a change in host cell viability.

156

157

158   **PD-1 pathway inhibition increases Mtb growth in the 3D model**

159   Having demonstrated that the PD-1/PD-L1 axis was up-regulated by infection in the 3D

160   model, we investigated whether inhibition of this interaction modulated host control of Mtb.

161   We initially studied chemical inhibitors of the PD-1/PD-L1 axis (Inhibitor 1, $C_{29}H_{33}NO_5$) and

162   found that blocking PD-1/PD-L1 binding increased Mtb growth in a dose-dependent manner

163   (Figure 3A). This effect occurred in both normoxia and hypoxia (Figure 3–figure supplement

164   1). No effect of PD-1 inhibition on cell survival was noted at day 7 or day 14, utilising two

165   different assays suited to each time point (Figure 3B and C). Next, we studied spartalizumab,

166   a humanised monoclonal antibody with high-affinity to PD-1 that blocks the interaction with

167   PD-L1 and PD-L2 (24). Consistent with the chemical inhibition, PD-1 pathway inhibition

168   using spartalizumab increased Mtb growth in normoxia in a dose-dependent manner (Figure

169   3D). Similarly, in hypoxia spartalizumab increased Mtb growth (Figure 3E). Microspheres

170   must be restored to normoxia to measure Mtb luminescence, and therefore a single time point

171   was analysed. Anti-PD-1 antibody treatment had no significant effect on cell survival in

172   either normoxia or hypoxia (Figure 3F).

173

174

175   **PD-1 inhibition increases secretion of multiple cytokines and growth factors**

176   To investigate the underlying mechanism whereby PD-1 inhibition leads to increased Mtb

177   growth, we studied secretion of cytokines, chemokines and growth factors by measuring

178   accumulation in the media around Mtb-infected microspheres by Luminex array. Mtb

179   infection increased secretion of numerous analytes (Figure 4–figure supplement 1), and

180   inhibition of PD-1/PD-L1 signalling further significantly augmented secretion of twelve

181   analytes compared to Mtb infection alone (Figure 4). A similar augmentation of analyte

182   secretion was observed in hypoxic microspheres (Figure 4–figure supplement 2). The twelve

183   analytes that were further increased above Mtb infection with concurrent PD-1 inhibition

184   were IL-4, IL-6, IL-10, IL-12, TNF-α, IL-1RA, MIP-1α, MIP-1β, RANTES, G-CSF, GM-

185   CSF and VEGF (individual concentrations, Figure 4–figure supplement 1). Anti-PD-1 alone

186   increased TNF-α secretion, although to a lesser effect than in combination with Mtb infection

187   (Figure 4–figure supplement 3).

188

189   **Exogenous TNF-α increases Mtb growth in microspheres**

190   To establish which of these factors might be associated with increased Mtb growth, we added

191   the significantly upregulated analytes either individually or in combination pools to 3D

192   microspheres in normoxia at "low" (Figure 5) and "high" concentrations (Figure 5–figure

193   supplement 1), as determined by the concentration measured in the secretion analysis. TNF-α

194   was the dominant cytokine that increased Mtb growth, with other cytokines only having a

195   minor effect (Figure 5A). Chemokines (RANTES, MIP-1α and MIP-1β) and growth factors

196   (G-CSF) had no significant effect, while GM-CSF significantly increasing Mtb growth, but

197   the effect was smaller than for TNF-α (Figure 5B). Additionally, the only cytokine

198   combination that had a significant effect on Mtb growth was the pro-inflammatory pool

199   containing TNF-α, IL-6 and IL-12 (Figure 5C). The addition of Th$_2$ cytokines, chemokines or

200   other growth factors had no significant effect (individual growth curves at "high"

201   concentration, Figure 5–figure supplement 1). Furthermore, TNF-α had a progressive dose-

202   dependent effect increasing Mtb growth within microspheres (Figure 5D).

203

204   To explore the effect of TNF-α further, we then generated microspheres incorporating

205   infected PBMC with and without anti-TNF-α neutralising antibodies. Consistent with our

206   initial observation, anti-TNF-α neutralising antibodies suppressed the TNF-mediated

207   increased Mtb growth, with a partial reduction at each concentration studied of two different

208   neutralising antibodies (Figure 5E and Figure 5–figure supplement 2). Exogenous TNF-α

209   modulated macrophage polarisation within microspheres, reducing CD80 expression at day 7

210   (Figure 5–figure supplement 3). Therefore, we next investigated whether anti-PD-1-induced

211   Mtb growth could be reversed by blocking TNF-α activity. Anti-PD-1 antibody treatment of

212   infected cells again augmented Mtb growth, and this increased growth could be reversed by

213   the incorporation of anti-TNF-α antibodies into the microspheres (Figure 5F). This confirms

214   that an excess of TNF-α is the primary driver of increased Mtb growth caused by PD-1

215   inhibition in the 3D model.

216

217   **TNF-α is highly expressed in TB granulomas and sputum TNF-α negatively correlates**

218   **with circulating PD-1 expression**

219   Finally, to establish the *in vivo* relevance of our cell culture model findings, we performed

220   immunohistochemical analysis of biopsies from patients with standard TB and anti-PD-1

221   associated TB. TNF-α was expressed within TB granulomas, with greater immunoreactivity

222   than control lung tissue at the excision margin of lung cancer (Figure 6A). Consistent with

223   our cell culture observations, TNF-α immunostaining was extensive in a biopsy from a

224   patient that developed pulmonary TB whilst treated with pembrolizumab, an anti-PD-1

225   antibody (Figure 6B). Quantitative analysis of differences between standard TB and anti-PD-

226 1 TB was not possible due to the unique nature of this clinical specimen, as TB diagnosis is

227 usually made by bronchoalveolar lavage as opposed to percutaneous biopsy.

228

229 We then analysed the association between PD-1 expression by circulating CD4$^+$ and CD8$^+$ T

230 cells and sputum TNF-α concentrations in a previously reported cohort (25). Although this

231 involved comparing PD-1 expression by circulating T cells, remote from the site of disease,

232 with total TNF-α concentration in the sputum, we hypothesised that a reverse association

233 would support the conclusion that PD-1 limits TNF-α secretion in patients. Consistent with

234 this, CD4$^+$ T cell PD-1 expression negatively correlated with sputum TNF-α, with a

235 significant negative association despite the relatively low sample numbers, which would be

236 expected to obscure an effect (Figure 6C).

237

238

239

240 **Discussion**

241 Although Mtb kills more people than any other infection worldwide, an enduring enigma is

242 that 90% of those exposed exert lifelong control of the pathogen. In seminal post-mortem

243 studies when TB was highly prevalent in the United States, Opie showed that 30% of humans

244 who died from other causes had viable Mtb present in the lung apices (26). Therefore, in the

245 majority of exposed individuals, a stable relationship forms between host immune cells and

246 Mtb without disease developing. Disseminated TB disease often develops in

247 immunocompromised individuals, such as advanced HIV infection, newborn infants or

248 following anti-TNF-α therapy, and this observation informs the view that TB can arise as a

249 disease of a deficient immune response to the pathogen (3).

250

251   However, the commonest form of human TB, and the one that leads to transmission, is apical

252   pulmonary disease (27). This occurs most frequently in young adults between the ages of 20-

253   25 with the strongest recall response to Mtb antigens, as measured by the Mantoux test (28).

254   Therefore, these clinical observations demonstrate that infection results in a stable symbiosis

255   between host and pathogen in the majority of individuals, and a pronounced immune

256   response associates with the subsequent development of infectious pulmonary disease. The

257   recently emerging clinical phenomenon of TB rapidly developing after initiating anti-PD-1

258   immunotherapy (5-15) further reinforces that an excessive immune response in TB can be

259   harmful.

260

261   PD-1 is expressed on T cells at the site of TB disease and PD-1 expression on circulating

262   CD4+ T cells associates with bacterial load (29). PD-1 expression is elevated in circulating

263   CD4 T cells in TB (30) and has been proposed to limit an effective host immune response.

264   Consequently PD-1 inhibition has been advanced as a therapeutic target to accelerate

265   clearance of infection (4, 30-34). However, from an evolutionary perspective, PD-1 is

266   proposed to limit immunopathology in the face of chronic antigenic stimulation (35).

267   Therefore, it is equally plausible, and indeed perhaps more logical, that PD-1/PD-L1 pathway

268   up-regulation in TB is a physiologically appropriate response to the persistent pathogen. We

269   found that hypoxia further up-regulated the PD-1/PD-L1/2 axis, consistent with hypoxia

270   increasing expression in cancer (19), and TB lesions are hypoxic both in model animals and

271   human lesions (18, 36). Analysis of the effect of hypoxia is complicated that both host and

272   pathogen physiology are altered, with hypoxia causing reduced Mtb growth (37-39) but also

273   causing diverse host physiological changes.   PD-1 may be particularly important in limiting

274   excessive inflammation and pathology in conditions of low oxygen tension. TB reactivation

275   following immune checkpoint blockade, and the extreme susceptibility of PD-1 deficient

276 mice to Mtb infection (16, 17), would support such a regulatory role, even though it runs

277 counter to widely advanced disease paradigms.

278

279 Our work further highlights the double-edged sword of the host immune response in TB (40).

280 TNF-α is clearly essential to an effective host immune response to TB, as disease frequently

281 develops after treatment with anti-TNF-α antibodies (41), and TNF-α inhibits Mtb growth in

282 zebrafish macrophages (42) and human alveolar macrophages (43). However, excessive

283 TNF-α is also associated with poor outcomes in TB. In human cells, an excess of TNF-α can

284 increase Mtb growth (44, 45), consistent with our observations. In patients with active TB,

285 TNF-α expression by Mtb-specific T cells is increased (46, 47) and TNF-α associates with

286 more severe radiological findings (48, 49). In diverse model systems, excessive TNF-α has

287 been shown to cause harmful inflammation (50-54), consistent with TNF-α exerting a bell-

288 shaped effect on host immunity, with either deficit or excess detrimental. Similarly, we report

289 a deleterious effect of additional GM-CSF, in contrast to GM-CSF improving control of Mtb

290 growth in murine macrophages (55). This suggests that cytokine responses are highly dose

291 and context dependent, potentially with each demonstrated non-linear responses leading to a

292 complex matrix of what may denote the optimal cytokine profile for Mtb control. Consistent

293 with our findings, in the one patient that developed TB on anti-PD-1 treatment where

294 longitudinal samples are available, there was a spike in PPD-specific TNF-α expressing cells

295 prior to with the development of active TB (13), consistent with PD-1 acting as a regulator of

296 TNF-α expression in TB. Taken together, these findings demonstrate a harmful effect of

297 excessive TNF-α in TB.

298

We found that multiple cytokines and chemokines were increased after PD-1 inhibition, and therefore events in humans are likely to be more complex than TNF-α excess alone. The augmented inflammation may have multiple harmful effects, such as recruitment of excessive inflammatory cells and destruction of the extracellular matrix (56-58), which favour Mtb growth. In the mouse model of TB, one key role of PD-1 is to limit IFN-γ production (59), and we have shown that excess IFN-γ also accelerates Mtb growth in microspheres (20). We did not show an effect of TNF-α on cell survival, although TNF-α has been reported to increase macrophage necrosis in the zebrafish model, via a mitochondrial-lysosomal-endoplasmic reticulum circuit (53, 60). The effect of PD-1 inhibition on macrophage polarisation and survival warrants further investigation, as this is likely to be one determinant of outcome (61, 62).

As in all *in vitro* systems, the bioelectrospray model has limitations (63). For example, it does not permit the ingress of new inflammatory cells, and therefore can only be used to investigate the early events resulting from anti-PD-1 treatment, and not the recruitment of inflammatory cells by increased chemokine secretion. In addition, although it permits longer analysis of the host-pathogen interaction than other human primary cell culture systems, the 3 week standard experiment remains shorter than human infection, and so it models early events. We have not yet characterised which cells which produce TNF-α, nor the wider phenotypic changes that result from inhibition of the PD-1 axis. The optimal approach would be to integrate single cell RNAseq to the analysis pipeline, so the phenotype of different cells can be comprehensively analysed. As microspheres can be readily dissolved by incubation in EDTA to release the cells, the system is suited for this technical development.

322   The common side effects of anti-PD-1 treatment in patients are termed immune related

323   Adverse Events (irAEs), which are autoimmune in nature (64). We have proposed that an

324   autoimmune process may exacerbate pathology in TB (65), and others have suggested that a

325   loss of tolerance underlies progression to active TB (66, 67). The common theme is that an

326   excessive response to antigens, whether host or pathogen-derived, can drive disease in TB

327   and our findings further support this conclusion. PD-1 may act to fine tune the balance

328   between pro- and anti-inflammatory responses necessary to control infection without causing

329   pathology. Notably, immune related adverse events to immune checkpoint inhibitors may be

330   treated with anti-TNF-α antibodies (64), suggesting TNF-α may be the primary driver of both

331   autoimmunity and TB pathology after PD-1 treatment.

332

333   Our model provides the mechanistic insights into a clinical phenomenon with significant

334   implications for future TB treatment and vaccine approaches. Simply driving a stronger

335   immune response to Mtb seems unlikely to be beneficial, as clinical and epidemiological data

336   suggest it may be harmful. For example, host-directed therapies may be designed to

337   accelerate bacterial clearance whilst concurrently reducing immunopathological effects by

338   appropriate skewing of macrophage phenotype. A more nuanced view considering the

339   different immunological phases of TB is essential, differentiating events at the point of initial

340   exposure from the late events at the apex of the lung, where excessive inflammation leads to

341   immunopathology and transmission (68). Defining the distinction between a protective and

342   pathological immune response in human TB remains a key unanswered question, essential to

343   inform new interventions to control the TB pandemic.

344

345

346   **Materials and Methods**

Key Resources Table				
Reagent type (species) or resource	**Designation**	**Source or reference**	**Identifiers**	**Additional information**
Strain, strain background (*Mycobacterium tuberculosis*)	H37Rv	(From Ref: 20)		Used at multiple of infection of 0.1
Strain, strain background (*Mycobacterium tuberculosis*)	H37Rv pMV306hsp+LuxAB+G13+CDE	(From Ref: 20)		Used at multiple of infection of 0.1
Strain, strain background (*Mycobacterium tuberculosis*)	H37Rv pMV306hsp encoding the wild-type FFluc	(From Ref: 20)		Used at multiple of infection of 0.1
Biological sample (Antibodies)				
Antibody	anti-CD45-V500 Horizon (Clone no. HI30)	BD Biosciences	Cat.No.563792	Monoclonal mouse antibody
Antibody	anti-CD3 Brilliant Violet 785 (Clone no. OKT3)	Biolegend	Cat.No.317330	Monoclonal mouse antibody
Antibody	anti-CD3-PE (Clone no. HIT3a)	Biolegend	Cat.No.300308	Monoclonal mouse antibody
Antibody	anti-CD4 Brilliant Ultra Violet 496 (Clone no. SK3)	BD Bioscience	Cat.No.612937	Monoclonal mouse antibody
Antibody	anti-CD4-PerCP (Clone no. OKT4)	Biolegend	Cat.No.317432	Monoclonal mouse antibody
Antibody	anti-CD8 Brilliant Violet 605 (Clone no. RPA-T8)	Biolegend	Cat.No.301040	Monoclonal mouse antibody
Antibody	anti-CD8-APC (Clone no. SK1)	Biolegend	Cat.No.344722	Monoclonal mouse antibody
Antibody	anti-CD103-APC (Clone no. Ber-ACT8)	BD Biosciences	Cat.No.563883	Monoclonal mouse antibody
Antibody	anti-CD69 Brilliant Ultra Violet 395 (Clone no. FN50)	Biolegend	Cat.No.310902	Monoclonal mouse antibody
Antibody	anti-HLA-DR-PerCP (Clone no. L243)	Biolegend	Cat.No.307628	Monoclonal mouse antibody
Antibody	anti-CD279-BB515 (Clone no. EH12.1)	BD Biosciences	Cat.No.564494	Monoclonal mouse antibody
Antibody	anti- CD-274-BB515 (Clone no. MIH1)	BD Biosciences	Cat.No.564554	Monoclonal mouse antibody
Antibody	anti-PD-1 Brilliant Violet 421 (Clone no.EH12.1)	BD Biosciences	Cat.No.562516	Monoclonal mouse antibody
Antibody	anti-CD11b-APC (Clone no. ICRF44)	Biolegend	Cat.No.301310	Monoclonal mouse antibody
Antibody	anti-CD45-APC/Cy7 (Clone no. 2D1)	Biolegend	Cat.No.368516	Monoclonal mouse antibody
Antibody	anti-CD14-AP/APC (Clone no. HCD14)	Biolegend	Cat.No.325608	Monoclonal mouse antibody
Antibody	anti-True-Stain Monocyte Blocker™	Biolegend	Cat.No.426102	Monoclonal mouse antibody
Antibody	anti-CD4 (Clone no. M7310)	DAKO	Cat.No.M7310	Monoclonal mouse antibody

Antibody	anti-CD8 (Clone no. M7103)	DAKO	Cat.No. M7103	Monoclonal mouse antibody
Antibody	anti-PD1 (Clone no. ab5287)	Abcam	Cat.No.ab52587	Monoclonal mouse antibody
Antibody	anti-TNF-α (Clone no. ab1793)	Abcam	Cat.No.ab1793	Monoclonal mouse antibody
Antibody	Spartalizumab	Selleckchem	Cat.No.A2017	20µg/ml and 200µg/ml, monoclonal , mouse IgG4
Antibody	IgG4	Sino Biologicals	Cat.No.13505-HNAH	20µg/ml and 200µg/ml,monoclonal , mouse IgG4
Antibody	Mouse IgG1 kappa Isotype Control (P3.6.2.8.1),	Thermo Fisher Scientific	Cat.No.16-4714-82	50 µg/ml, mouse monoclonal IgG2A
Antibody	Mouse IgG1 Negative Control, clone Ci4	Merck Life Sciences	Cat.No.MABC002	51 µg/ml, mouse monoclonal IgG2A
Antibody	anti-TNF-α	Thermo Fisher Scientific	Cat.No.16-7348-81	52 µg/ml, mouse monoclonal IgG2A
Sequence-based reagent (Applied Biosystems TaqMan Gene Expression primers)	GAPDH	Thermo Fisher Scientific	#Hs02758991_g1	
	β2-Microbulin	Thermo Fisher Scientific	#Hs00608023_m1	
	FNTA	Thermo Fisher Scientific	#Hs00357739_m1	
	PDCD1	Thermo Fisher Scientific	#Hs01550088_m1	
	CD274	Thermo Fisher Scientific	#Hs00204257_m1	
	PDCD1LG2	Thermo Fisher Scientific	#Hs00228839_m1	
	HIF-1α	Thermo Fisher Scientific	#Hs00153153_m1	
Commercial assay or kit	CytoTox-Glo Cytotoxicity Assay	Promega	G9291	Commercial assay or kit
	Lactate Dehydrogenase Activity Assay Kit	Merck	11 644 793 001	Commercial assay or kit
	Cytokine and Chemokine 35-Plex Human ProcartaPlex™ Panel	Thermo Fisher Scientific	LHC6005M	Commercial assay or kit
Chemical compound, drug	PD-1/PD-L1 Inhibitor 1	Cambridge Biosciences, UK	#1675201-83-8	Chemical compound
	Recombinant Human G-CSF	ImmunoTools	Cat.No.11343115	1 ng/ml and 5 ng/ml

	Recombinant Human GM-CSF	ImmunoTools	Cat.No.11343125	0.25 ng/ml and 1.25 ng/ml
	Recombinant Human IL-1RA / IL1F3	ImmunoTools	Cat.No.11344876	1.25 ng/ml and 6.25 ng/ml
	Recombinant Human IL-10	ImmunoTools	Cat.No.11340105	0.2 ng/ml and 1 ng/ml
	Recombinant Human IL-6	ImmunoTools	Cat.No.11340066	10.0 ng/ml and 50.0 ng/ml
	Recombinant Human IL-12	ImmunoTools	Cat.No.11349125	0.5 ng/ml and 2.5 ng/ml
	Recombinant Human TNF-α	ImmunoTools	Cat.No.11343017	0.3 ng/ml , 1.5 ng/ml, 7.5ng/ml and 15ng/ml
	Recombinant Human IL-15	ImmunoTools	Cat.No.11340155	0.5ng/ml, 5ng/ml and 50ng/ml
	Recombinant Human IL-17A	ImmunoTools	Cat.No.11340176	1 ng/ml , 10ng/ml and 100ng/ml
	Recombinant Human IL-17F	ImmunoTools	Cat.No.11349176	1 ng/ml , 10ng/ml and 100ng/ml
	Recombinant Human RANTES	ImmunoTools	Cat.No.11343196	0.3 ng/ml and 1.5 ng/ml
	Recombinant Human MIP-1α	ImmunoTools	Cat.No.11343206	1.5 ng/ml and 7.5 ng/ml
	Recombinant Human MIP-1β	ImmunoTools	Cat.No.11343223	1.0 ng/ml and 5 ng/ml
	Recombinant Human MCP	ImmunoTools	Cat.No.11343386	1 ng/ml , 10ng/ml and 100ng/ml
Software, algorithm	FlowJo	BD Bioscences	version 10.6.1	Software
	BD FACSDiva™ Software	BD Biosciences		Software
	Graphpad Prism	GraphPad Software LLC	v7.05	Software

347

M. tuberculosis culture

M. tuberculosis H37Rv (Mtb) was cultured in Middlebrook 7H9 medium (supplemented with 10% ADC, 0.2% glycerol and 0.02% Tween 80) (BD Biosciences, Oxford). Bioluminescent Mtb containing luxABCDE (Mtb lux+) and Mtb expressing ffLuc (Mtb ffLuc+) were cultured with kanamycin 25μg/ml. Luminescence was measured with either GloMax® 20/20 single tube luminometer (Promega,UK) or GloMax® Discover microplate reader (Promega,UK). Cultures at $1x\ 10^8$ CFU/ml Mtb (OD= 0.6) were used for all experiments at multiplicity of infection (MOI) of 0.1. Live Mtb was used in all experiments apart from the time lapse microscopy, which used UV killed TB. Mtb colony counting was performed by serial dilution on Middlebrook 7H11 Agar. Bioluminescence from the Mtb ffLuc+ was induced using D-luciferin (ThermoFisher, UK) at a concentration of 750μM in Hank's balanced salt solution (HBSS).

PBMC cell isolation from human blood

For the 3D microsphere experiments, PBMC were separated from single donor leukocyte cones (National Health Service Blood and Transfusion, Southampton, UK) by density gradient centrifugation over Ficoll-Paque (GE Healthcare Life Sciences). Ethical approval for these studies was provided by the National Research Ethics Service Committee South Central - Southampton A, ref 13/SC/0043.

Study participants for the correlation analysis of sputum-TNF-α with PD-1 expression on $CD4^+$ and $CD8^+$ T cells are the cross-sectional study individuals in a previously reported cohort (25, 69). Participants were recruited from an outpatient clinic in Khayelitsha, South Africa and were either healthy volunteers, non-TB respiratory symptomatics or recently diagnosed TB patients. Flow cytometric analysis was performed on cryopreserved PBMC isolated from whole blood as previously reported (69). The study was approved by the

372 University of Cape Town Human Research Ethics Committee (REF 516/2011) and conducted

373 in accordance with the Declaration of Helsinki.

Analysis of PD-1 expression in blood and lung of TB patients

375 Lung tissue and matched PBMC were obtained from the AHRI Lung study cohort approved

376 by the Biomedical Research Ethics Committee (BREC) of the University of Kwa-Zulu Natal,

377 BREC reference: BE019/13. All participants underwent surgical resection to treat TB related

378 lung complications, including haemoptysis, bronchiectasis, persistent cavitatory disease,

379 shrunken or collapsed lung or drug-resistant infection, at the King Dinuzulu Hospital in

380 Durban, KwaZulu- Natal and Inkosi Albert Luthuli Central Hospital (IALCH) in Durban,

381 KwaZulu-Natal. PBMC were isolated from whole blood using standard Ficoll-Histopaque

382 (Sigma) density gradient centrifugation by standard protocol.

383 Lung tissues was cut into approximately $1mm^3$ pieces, washed several times with cold HBSS

384 (Lonza) and re-suspended in 8mls of pre-warmed digestion media R10 (RPMI supplemented

385 with 10% FCS, 2 mM L-glutamate, 100 U/ml Penstrep), containing 0.5 mg/ml collagenase D

386 (Roche) and 40 U/ml DNaseI (Roche), and transferred to GentleMACS C-tubes (Miltenyi)

387 for mechanical digestion according to the manufacturer's instructions. The suspension was

388 incubated for 30 minutes at 37° C, followed by an additional mechanical digestion step and

389 another 30-minute incubation step at 37^oC. The final suspension was passed through a 70 μm

390 cell strainer and washed twice in HBSS. PBMC and lung cells were phenotyped by surface

391 staining with a near-infrared live/dead cell viability cell staining kit (Invitrogen) and a

392 cocktail of fluorochrome conjugated antibodies: αCD45-V500 Horizon clone HI30 (BD

393 Biosciences), αCD3 Brilliant Violet 785 clone OKT3 (Biolegend), αCD4 Brilliant Ultra

394 Violet 496 clone SK3 (BD Bioscience), αCD8 Brilliant Violet 605 clone RPA-T8

395 (Biolegend), αCD103-APC clone Ber-ACT8 (BD Biosciences), αCD69 Brilliant Ultra Violet

395 clone FN50 (Brilliant Horizon), αPD-1 Brilliant Violet 421 clone EH12.1 (BD

Biosciences). Cells were stained with 25uL of antibody cocktail in the dark for 20 minutes at

room temperature followed by washing with PBS, then fixed in 2% PFA. Data was acquired

using BD Aria Fusion cytometer and analyzed using FlowJo Software v.9.9 (Treestar Inc,

Ashland, OR).

Immunohistochemistry of paraffin-fixed tissue

Immunohistochemical analysis was performed on paraffin-embedded lung tissue from

patients with pulmonary TB and lung cancer that were mounted at 4μm thin onto APS coated

glass slides and dried, using the following antibodies: anti-CD4 (Clone no. M7310) (DAKO),

anti-CD8 (Clone no. M7103) (DAKO), anti-PD1 (Clone no. ab5287) (Abcam) and anti-TNF-

α (Clone no. ab1793) (Abcam). Staining was done at optimised concentrations

usingrecommended buffers for each antibody.

Microencapsulation of cells

Microspheres were generated with an electrostatic generator (Nisco, Zurich, Switzerland) as

described previously (1). Briefly, PBMC were infected overnight with Mtb in a $250cm^2$ flask,

cells were detached, pelleted and mixed with 1.5% sterile alginate (Pronova UP MVG

alginate, Nova Matrix, Norway) and 1mg/mL collagen (Advanced BioMatrix, USA) at a final

concentration of 5×10^6 cells/ml. The cell-alginate suspension was injected into the bead

generator where microspheres were formed in an ionotropic gelling bath of 100mM $CaCl_2$ in

HBSS. After washing twice with HBSS with Ca^{2+}/Mg^{2+}, microspheres were transferred in

RPMI 1640 medium containing 10% human AB serum and incubated at 37^oC. Microspheres

were either dispensed into eppendorfs, which were then randomly allocated to different

environmental conditions, or plated into a 96-well plate with conditions in triplicate

according to a pre-determined template. For experiments in hypoxia, microspheres were

420   incubated in 1% oxygen in Galaxy 48 R CO_2 incubator (Eppendorf, UK) until analysis.

421   Supernatants were collected at defined time points. Time points described are days post

422   infection.

423   **Live Cell Imaging**

424   Uninfected or UV killed Mtb infected cells suspended in alginate-collagen matrix were plated

425   in an 8 well μ-Slide (ibidi GmbH, Germany). HBSS containing Ca^{2+} was used for cross-

426   linking of alginate in the extracellular matrix for 15 minutes and then replaced with RPMI

427   medium with 10% human AB serum. Samples were imaged using an Olympus IX81 time-

428   lapse microscope with temperature of 37°C and CO_2 concentration 5%. Z-stacks 200 μm in

429   height were captured at one position in each sample every 30 minutes for 48 hours. Images

430   were exported as tif files and opened in ImageJ.

431   **PD-1/PD-L1 Inhibition**

432   Small chemical inhibition of PD-1/PD-L1 signalling was by PD-1/PD-L1 Inhibitor 1 (CAS

433   Registry #1675201-83-8, Cambridge Biosciences, UK), a compound that competitively

434   blocks the interaction of PD-1 with it ligand protein PD-L1 (70). Inhibitor 1 was prepared in

435   DMSO (Sigma-Aldrich,UK) at a concentration of 6.3mM and dissolved to a concentration of

436   1nM, 10nM, 100nM and 1μM in complete media and added to media around microspheres on

437   the day after encapsulation. Luminescence was monitored on specific days. For the

438   microspheres incubated in hypoxic conditions, measurement of luminescence was repeated

439   for every 30 minutes after the addition of luciferin until the reading plateaued, which was

440   usually 2 hrs.

441   In antibody inhibitory experiments, spartalizumab (Selleckchem, Germany), a humanised

442   IgG4 anti-PD1 monoclonal antibody, was used to inhibit of PD-1/PD-L1 signalling in

443   microspheres. Briefly, cells were infected with Mtb overnight, pelleted and then a suspension

444   of anti-PD1 antibodies (20 and 200μg/ml) were added and pre-incubated for 1 hour. Cells

445   were then encapsulated within microspheres and kept for 14 days in either normoxia or 1%

446   oxygen at 37°C and 5% CO_2. Mtb growth was measured using luminescence and

447   supernatants were taken for either cytokine or LDH measurement. An IgG4 human antibody

448   was used at the same concentration as a control.

449   **Cell Toxicity Assays**

450   Lactate dehydrogenase (LDH) release in the supernatants collected at different time points

451   was analysed by a colorimetric activity assay as per manufacturer's instructions (Roche,

452   Burgess Hill, United Kingdom). As a second assay, CytoTox-Glo Cytotoxicity Assay

453   (Promega) was used, which measures dead-cell protease activity released from cells without

454   membrane integrity using a luminogenic peptide substrate, the AAF-Glo™ Substrate.

455   Luminescence from 96-well plates was analysed by GloMax Discover (Promega). The LDH

456   assay was suited for later time points, as this could be performed on microspheres in

457   eppendorfs, while the CytoTox glow required analysis in 96 well plates and so was best

458   suited to analysis in the first week.

459   **Gene Expression Analysis**

460   All the reagents were sourced from ThermoFisher Scientific (Paisley, UK). In brief,

461   microspheres were decapsulated with 5mM EDTA, cells were pelleted and immediately lysed

462   using TRIzol Reagent. RNA was transcribed using High Capacity cDNA Reverse

463   Transcription kit. TaqMan® Universal master mix and primers specific for genes were

464   GAPDH (#Hs02758991_g1), β2-Microbulin (#Hs00608023_m1), FNTA

465   (#Hs00357739_m1), PDCD1 (#Hs01550088_m1), CD274 (#Hs00204257_m1), PDCD1LG2

466   (#Hs00228839_m1) and HIF-1α (Hs00153153_m1) were used for qPCR according to the

467 manufacturer's instructions and the comparative threshold (CT) method was employed to

468 analyse all qPCR data.

Immunophenotyping of cells from microspheres

470 Microspheres were decapsulated with 5mM EDTA in HBSS with no Ca^{2+}/Mg^{2+} at day 7 after

471 encapsulation and 2 million cells prepared for staining in RPMI with 5% foetal bovine serum.

472 To measure the expression of PD-1 in $CD4^+$ and $CD8^+$ T cells and PD-L1 expression in

473 $CD14^+CD11b^+$ cells, the following antibody panel was used: CD3-PE (clone HIT3a,

474 Biolegend), HLA-DR-PerCP (clone L243, Biolegend), CD4-PerCP (clone OKT4,

475 Biolegend), CD8-APC (clone SK1, Biolegend), CD11b-APC (clone ICRF44, Biolegend),

476 CD45-APC/Cy7 (clone 2D1, Biolegend), CD14-AP/APC (clone HCD14, Biolegend),

477 CD279-BB515 (Clone EH12.1, BD), CD-274-BB515 (Clone MIH1, BD) and True-Stain

478 Monocyte Blocker™ (Biolegend, USA). Gates were defined using fluorescence minus one

479 control after exclusion of the dead cells using Live/Dead fixable stain (ThermoFisher, UK).

480 Gating strategy is provided in Figure 5–figure supplement 4. Cells were acquired after fixing

481 them in 2% paraformaldehyde in HBSS for 1 hour using FACSAria (Becton Dickinson, UK)

482 and analysed by FACSDiva software (Becton Dickinson) and Flow Jo version 10 (Treestar).

Cytokine supplementation

484 Microspheres were incubated in RPMI 1640 with 10% AB serum in an opaque 12-well tissue

485 culture plate with G-CSF, GM-CSF, IL-1RA, IL-6, IL-10, IL-12, IL-15, IL-17A, IL-17F,

486 TNF-α, RANTES, MIP-1α, MIP-1β and MCP at two concentrations determined by the

487 cellular experiments, at 37°C and 5% CO_2. All the cytokines were purchased from

488 ImmunoTools (Germany), suspended in RPMI with 0.1% human serum and kept at -80^OC

489 until use. Bacterial growth was monitored with luminescence using GloMax® Discover

490 microplate reader (Promega,UK).

Luminex Analysis

Samples were sterilised by filtration through a 0.22μM Durapore membrane (MerkMillipore). Concentrations of cytokines (ThermoFisher, UK) were determined using a Bioplex 200 platform (Bio-Rad, UK) according to the manufacturer's protocol and quantified per milligram of total protein measured by Bradford assay (Biorad).

Statistical analysis

All experiments were performed on a minimum of 2 occasions from separate donors as biological replicates and on each occasion with a minimum of 3 technical replicates. Some donor-to-donor variation occurred in terms of absolute RLU, as expected in the analysis of primary human cells, but the direction of effects were always consistent. Data presented are from a representative donor and include the mean and SEM. Analysis was performed in Graphpad Prism v7.05. Students t-test was used to compare pairs and ANOVA with Tukey's correction for multiple comparisons for groups of 3 or more groups where it was appropriate. For the flow cytometric analysis of clinical samples, data were analysed using Mann-Whitney test for comparing pairs and Kruskal-Wallis test with Dunn's multiple comparisons test for 3 or more group.

References

1. Wallis RS, Maeurer M, Mwaba P, Chakaya J, Rustomjee R, Migliori GB, et al. Tuberculosis-advances in development of new drugs, treatment regimens, host-directed therapies, and biomarkers. Lancet Infect Dis. 2016;16(4):e34-46.

2. Menardo F, Duchêne S, Brites D, Gagneux S. The molecular clock of Mycobacterium tuberculosis. PLoS pathogens. 2019;15(9):e1008067.

3. O'Garra A, Redford PS, McNab FW, Bloom CI, Wilkinson RJ, Berry MP. The immune response in tuberculosis. Annu Rev Immunol. 2013;31:475-527.

4. Zumla A, Rao M, Wallis RS, Kaufmann SH, Rustomjee R, Mwaba P, et al. Host-directed therapies for infectious diseases: current status, recent progress, and future prospects. Lancet Infect Dis. 2016;16(4):e47-63.

5. Fujita K, Terashima T, Mio T. Anti-PD1 Antibody Treatment and the Development of Acute Pulmonary Tuberculosis. J Thorac Oncol. 2016;11(12):2238-40.

6. Lee JJ, Chan A, Tang T. Tuberculosis reactivation in a patient receiving anti-programmed death-1 (PD-1) inhibitor for relapsed Hodgkin's lymphoma. Acta Oncol. 2016;55(4):519-20.

7. Chu YC, Fang KC, Chen HC, Yeh YC, Tseng CE, Chou TY, et al. Pericardial Tamponade Caused by a Hypersensitivity Response to Tuberculosis Reactivation after Anti-PD-1 Treatment in a Patient with Advanced Pulmonary Adenocarcinoma. J Thorac Oncol. 2017;12(8):e111-e4.

8. Picchi H, Mateus C, Chouaid C, Besse B, Marabelle A, Michot JM, et al. Infectious complications associated with the use of immune checkpoint inhibitors in oncology: reactivation of tuberculosis after anti PD-1 treatment. Clinical Microbiology and Infection. 2018;24(3):216-8.

9. Jensen KH, Persson G, Bondgaard AL, Pohl M. Development of pulmonary tuberculosis following treatment with anti-PD-1 for non-small cell lung cancer. Acta Oncol. 2018;57(8):1-2.

10. Elkington PT, Bateman AC, Thomas GJ, Ottensmeier CH. Implications of Tuberculosis Reactivation after Immune Checkpoint Inhibition. Am J Respir Crit Care Med. 2018;198(11):1451-3.

550   11.   He W, Zhang X, Li W, Kong C, Wang Y, Zhu L, et al. Activated pulmonary tuberculosis in a

551   patient with melanoma during PD-1 inhibition: a case report. Onco Targets Ther. 2018;11:7423-7.

552   12.   Takata S, Koh G, Han Y, Yoshida H, Shiroyama T, Takada H, et al. Paradoxical response in a

553   patient with non-small cell lung cancer who received nivolumab followed by anti-Mycobacterium

554   tuberculosis agents. J Infect Chemother. 2019;25(1):54-8.

555   13.   Barber DL, Sakai S, Kudchadkar RR, Fling SP, Day TA, Vergara JA, et al. Tuberculosis

556   following PD-1 blockade for cancer immunotherapy. Sci Transl Med. 2019;11(475).

557   14.   Tsai CC, Chen JH, Wang YC, Chang FY. Re-activation of pulmonary tuberculosis during

558   anti-programmed death-1 (PD-1) treatment. QJM. 2019;112(1):41-2.

559   15.   van Eeden R, Rapoport BL, Smit T, Anderson R. Tuberculosis Infection in a Patient Treated

560   With Nivolumab for Non-small Cell Lung Cancer: Case Report and Literature Review. Front Oncol.

561   2019;9:659.

562   16.   Lazar-Molnar E, Chen B, Sweeney KA, Wang EJ, Liu W, Lin J, et al. Programmed death-1

563   (PD-1)-deficient mice are extraordinarily sensitive to tuberculosis. Proc Natl Acad Sci U S A.

564   2010;107(30):13402-7.

565   17.   Barber DL, Mayer-Barber KD, Feng CG, Sharpe AH, Sher A. CD4 T cells promote rather

566   than control tuberculosis in the absence of PD-1-mediated inhibition. J Immunol. 2011;186(3):1598-

567   607.

568   18.   Belton M, Brilha S, Manavaki R, Mauri F, Nijran K, Hong YT, et al. Hypoxia and tissue

569   destruction in pulmonary TB. Thorax. 2016;71(12):1145-53.

570   19.   Noman MZ, Desantis G, Janji B, Hasmim M, Karray S, Dessen P, et al. PD-L1 is a novel

571   direct target of HIF-1alpha, and its blockade under hypoxia enhanced MDSC-mediated T cell

572   activation. J Exp Med. 2014;211(5):781-90.

573   20.   Tezera LB, Bielecka MK, Chancellor A, Reichmann MT, Shammari BA, Brace P, et al.

574   Dissection of the host-pathogen interaction in human tuberculosis using a bioengineered 3-

575   dimensional model. eLife. 2017;6:e21283.

576 21. Snyder ME, Finlayson MO, Connors TJ, Dogra P, Senda T, Bush E, et al. Generation and

577 persistence of human tissue-resident memory T cells in lung transplantation. Science Immunology.

578 2019;4(33):eaav5581.

579 22. Tezera LB, Bielecka MK, Elkington PT. Bioelectrospray Methodology for Dissection of the

580 Host-pathogen Interaction in Human Tuberculosis. Bio Protoc. 2017;7(14).

581 23. Egen JG, Rothfuchs AG, Feng CG, Winter N, Sher A, Germain RN. Macrophage and T Cell

582 Dynamics during the Development and Disintegration of Mycobacterial Granulomas. Immunity.

583 2008;28(2):271-84.

584 24. Kaplon H, Reichert JM. Antibodies to watch in 2019. mAbs. 2019;11(2):219-38.

585 25. Walker NF, Wilkinson KA, Meintjes G, Tezera LB, Goliath R, Peyper JM, et al. Matrix

586 Degradation in Human Immunodeficiency Virus Type 1-Associated Tuberculosis and Tuberculosis

587 Immune Reconstitution Inflammatory Syndrome: A Prospective Observational Study. Clin Infect Dis.

588 2017;65(1):121-32.

589 26. Opie EL, Aronson JD. Tubercle bacilli in latent tuberculous lesions and in lung tissue without

590 tuberculous lesions. Arch Pathol Lab Med. 1927;4(1):1-21.

591 27. Elkington PT, D'Armiento JM, Friedland JS. Tuberculosis immunopathology: the neglected

592 role of extracellular matrix destruction. Sci Transl Med. 2011;3(71):71ps6.

593 28. Comstock GW, Livesay VT, Woolpert SF. The prognosis of a positive tuberculin reaction in

594 childhood and adolescence. American journal of epidemiology. 1974;99(2):131-8.

595 29. Day CL, Abrahams DA, Bunjun R, Stone L, de Kock M, Walzl G, et al. PD-1 Expression on

596 Mycobacterium tuberculosis-Specific CD4 T Cells Is Associated With Bacterial Load in Human

597 Tuberculosis. Frontiers in immunology. 2018;9:1995.

598 30. Shen L, Gao Y, Liu Y, Zhang B, Liu Q, Wu J, et al. PD-1/PD-L pathway inhibits M.tb-

599 specific CD4(+) T-cell functions and phagocytosis of macrophages in active tuberculosis. Sci Rep.

600 2016;6:38362.

601 31. Jurado JO, Alvarez IB, Pasquinelli V, Martinez GJ, Quiroga MF, Abbate E, et al.

602 Programmed death (PD)-1:PD-ligand 1/PD-ligand 2 pathway inhibits T cell effector functions during

603 human tuberculosis. J Immunol. 2008;181(1):116-25.

604   32.   Singh A, Mohan A, Dey AB, Mitra DK. Inhibiting the programmed death 1 pathway rescues

605   Mycobacterium tuberculosis-specific interferon gamma-producing T cells from apoptosis in patients

606   with pulmonary tuberculosis. J Infect Dis. 2013;208(4):603-15.

607   33.   Suarez GV, Melucci Ganzarain CDC, Vecchione MB, Trifone CA, Marin Franco JL, Genoula

608   M, et al. PD-1/PD-L1 Pathway Modulates Macrophage Susceptibility to Mycobacterium tuberculosis

609   Specific CD8(+) T cell Induced Death. Sci Rep. 2019;9(1):187.

610   34.   Jiang J, Wang X, An H, Yang B, Cao Z, Liu Y, et al. Mucosal-associated invariant T-cell

611   function is modulated by programmed death-1 signaling in patients with active tuberculosis. Am J

612   Respir Crit Care Med. 2014;190(3):329-39.

613   35.   Sharpe AH, Pauken KE. The diverse functions of the PD1 inhibitory pathway. Nat Rev

614   Immunol. 2018;18(3):153-67.

615   36.   Via LE, Lin PL, Ray SM, Carrillo J, Allen SS, Eum SY, et al. Tuberculous granulomas are

616   hypoxic in guinea pigs, rabbits, and nonhuman primates. Infect Immun. 2008;76(6):2333-40.

617   37.   Devasundaram S, Gopalan A, Das SD, Raja A. Proteomics Analysis of Three Different

618   Strains of Mycobacterium tuberculosis under In vitro Hypoxia and Evaluation of Hypoxia Associated

619   Antigen's Specific Memory T Cells in Healthy Household Contacts. Frontiers in microbiology.

620   2016;7:1275-.

621   38.   Ortega C, Liao R, Anderson LN, Rustad T, Ollodart AR, Wright AT, et al. Mycobacterium

622   tuberculosis Ser/Thr Protein Kinase B Mediates an Oxygen-Dependent Replication Switch. PLOS

623   Biology. 2014;12(1):e1001746.

624   39.   Eoh H, Rhee KY. Multifunctional essentiality of succinate metabolism in adaptation to

625   hypoxia in Mycobacterium tuberculosis. Proceedings of the National Academy

626   of Sciences. 2013;110(16):6554.

627   40.   Ehlers S. Immunity to tuberculosis: a delicate balance between protection and pathology.

628   FEMS Immunol Med Microbiol. 1999;23(2):149-58.

629   41.   Keane J, Gershon S, Wise RP, Mirabile-Levens E, Kasznica J, Schwieterman WD, et al.

630   Tuberculosis associated with infliximab, a tumor necrosis factor alpha-neutralizing agent. N Engl J

631   Med. 2001;345(15):1098-104.

632   42.   Clay H, Volkman HE, Ramakrishnan L. Tumor necrosis factor signaling mediates resistance

633   to mycobacteria by inhibiting bacterial growth and macrophage death. Immunity. 2008;29(2):283-94.

634   43.   Hirsch CS, Ellner JJ, Russell DG, Rich EA. Complement receptor-mediated uptake and tumor

635   necrosis factor-alpha-mediated growth inhibition of Mycobacterium tuberculosis by human alveolar

636   macrophages. The Journal of Immunology. 1994;152(2):743.

637   44.   Byrd TF. Tumor necrosis factor alpha (TNFalpha) promotes growth of virulent

638   Mycobacterium tuberculosis in human monocytes iron-mediated growth suppression is correlated

639   with decreased release of TNFalpha from iron-treated infected monocytes. J Clin Invest.

640   1997;99(10):2518-29.

641   45.   Engele M, Stossel E, Castiglione K, Schwerdtner N, Wagner M, Bolcskei P, et al. Induction

642   of TNF in human alveolar macrophages as a potential evasion mechanism of virulent Mycobacterium

643   tuberculosis. J Immunol. 2002;168(3):1328-37.

644   46.   Harari A, Rozot V, Enders FB, Perreau M, Stalder JM, Nicod LP, et al. Dominant TNF-

645   alpha+ Mycobacterium tuberculosis-specific CD4+ T cell responses discriminate between latent

646   infection and active disease. Nat Med. 2011;17(3):372-6.

647   47.   Tebruegge M, Dutta B, Donath S, Ritz N, Forbes B, Camacho-Badilla K, et al. Mycobacteria-

648   Specific Cytokine Responses Detect Tuberculosis Infection and Distinguish Latent from Active

649   Tuberculosis. Am J Respir Crit Care Med. 2015;192(4):485-99.

650   48.   Casarini M, Ameglio F, Alemanno L, Zangrilli P, Mattia P, Paone G, et al. Cytokine levels

651   correlate with a radiologic score in active pulmonary tuberculosis. Am J Respir Crit Care Med.

652   1999;159(1):143-8.

653   49.   Tsao TC, Hong J, Li LF, Hsieh MJ, Liao SK, Chang KS. Imbalances between tumor necrosis

654   factor-alpha and its soluble receptor forms, and interleukin-1beta and interleukin-1 receptor antagonist

655   in BAL fluid of cavitary pulmonary tuberculosis. Chest. 2000;117(1):103-9.

656   50.   Bekker LG, Moreira AL, Bergtold A, Freeman S, Ryffel B, Kaplan G. Immunopathologic

657   effects of tumor necrosis factor alpha in murine mycobacterial infection are dose dependent. Infect

658   Immun. 2000;68(12):6954-61.

659   51.   Taylor JL, Ordway DJ, Troudt J, Gonzalez-Juarrero M, Basaraba RJ, Orme IM. Factors

660   associated with severe granulomatous pneumonia in Mycobacterium tuberculosis-infected mice

661   vaccinated therapeutically with hsp65 DNA. Infect Immun. 2005;73(8):5189-93.

662   52.   Tsenova L, Bergtold A, Freedman VH, Young RA, Kaplan G. Tumor necrosis factor alpha is

663   a determinant of pathogenesis and disease progression in mycobacterial infection in the central

664   nervous system. Proc Natl Acad Sci U S A. 1999;96(10):5657-62.

665   53.   Roca FJ, Ramakrishnan L. TNF dually mediates resistance and susceptibility to mycobacteria

666   via mitochondrial reactive oxygen species. Cell. 2013;153(3):521-34.

667   54.   Tzelepis F, Blagih J, Khan N, Gillard J, Mendonca L, Roy DG, et al. Mitochondrial

668   cyclophilin D regulates T cell metabolic responses and disease tolerance to tuberculosis. Sci Immunol.

669   2018;3(23).

670   55.   Rothchild AC, Jayaraman P, Nunes-Alves C, Behar SM. iNKT Cell Production of GM-CSF

671   Controls Mycobacterium tuberculosis. PLoS Pathog. 2014;10(1):e1003805.

672   56.   Cambier CJ, O'Leary SM, O'Sullivan MP, Keane J, Ramakrishnan L. Phenolic Glycolipid

673   Facilitates Mycobacterial Escape from Microbicidal Tissue-Resident Macrophages. Immunity.

674   2017;47(3):552-65 e4.

675   57.   Al Shammari B, Shiomi T, Tezera L, Bielecka MK, Workman V, Sathyamoorthy T, et al. The

676   Extracellular Matrix Regulates Granuloma Necrosis in Tuberculosis. J Infect Dis. 2015;212(3):463-

677   73.

678   58.   Mishra BB, Lovewell RR, Olive AJ, Zhang G, Wang W, Eugenin E, et al. Nitric oxide

679   prevents a pathogen-permissive granulocytic inflammation during tuberculosis. Nat Microbiol.

680   2017;2:17072.

681   59.   Sakai S, Kauffman KD, Sallin MA, Sharpe AH, Young HA, Ganusov VV, et al. CD4 T Cell-

682   Derived IFN-gamma Plays a Minimal Role in Control of Pulmonary Mycobacterium tuberculosis

683   Infection and Must Be Actively Repressed by PD-1 to Prevent Lethal Disease. PLoS Pathog.

684   2016;12(5):e1005667.

685   60.   Roca FJ, Whitworth LJ, Redmond S, Jones AA, Ramakrishnan L. TNF Induces Pathogenic

686   Programmed Macrophage Necrosis in Tuberculosis through a Mitochondrial-Lysosomal-Endoplasmic

687   Reticulum Circuit. Cell. 2019;178(6):1344-61 e11.

688   61.   Lerner TR, Borel S, Greenwood DJ, Repnik U, Russell MR, Herbst S, et al. Mycobacterium

689   tuberculosis replicates within necrotic human macrophages. J Cell Biol. 2017;216(3):583-94.

690   62.   Cronan MR, Beerman RW, Rosenberg AF, Saelens JW, Johnson MG, Oehlers SH, et al.

691   Macrophage Epithelial Reprogramming Underlies Mycobacterial Granuloma Formation and Promotes

692   Infection. Immunity. 2016;45(4):861-76.

693   63.   Elkington P, Lerm M, Kapoor N, Mahon R, Pienaar E, Huh D, et al. In Vitro Granuloma

694   Models of Tuberculosis: Potential and Challenges. The Journal of infectious diseases.

695   2019;219(12):1858-66.

696   64.   Postow MA, Sidlow R, Hellmann MD. Immune-Related Adverse Events Associated with

697   Immune Checkpoint Blockade. N Engl J Med. 2018;378(2):158-68.

698   65.   Elkington P, Tebruegge M, Mansour S. Tuberculosis: An Infection-Initiated Autoimmune

699   Disease? Trends Immunol. 2016;37(12):815-8.

700   66.   Divangahi M, Khan N, Kaufmann E. Beyond Killing Mycobacterium tuberculosis: Disease

701   Tolerance. Frontiers in immunology. 2018;9:2976.

702   67.   Olive AJ, Sassetti CM. Tolerating the Unwelcome Guest; How the Host Withstands Persistent

703   Mycobacterium tuberculosis. Frontiers in immunology. 2018;9:2094.

704   68.   Elkington PT, Friedland JS. Permutations of time and place in tuberculosis. Lancet Infect Dis.

705   2015;15(11):1357-60.

706   69.   Walker NF, Opondo C, Meintjes G, Jhilmeet N, Friedland JS, Elkington PT, et al. Invariant

707   Natural Killer T cell dynamics in HIV-associated tuberculosis. Clin Infect Dis. 2019.

708   70.   Guzik K, Zak KM, Grudnik P, Magiera K, Musielak B, Törner R, et al. Small-Molecule

709   Inhibitors of the Programmed Cell Death-1/Programmed Death-Ligand 1 (PD-1/PD-L1) Interaction

710   via Transiently Induced Protein States and Dimerization of PD-L1. Journal of Medicinal Chemistry.

711   2017;60(13):5857-67.

712

713

Figure Legends

Figure 1: PD-1 is expressed in human TB granulomas. (A) Analysis of PD-1 expression by T cells in the lung and peripheral circulation of thirty-five TB patients undergoing medically indicated lung resection. PD-1 shows a trend towards higher expression by lung CD4$^+$ (i) and is significantly higher on lung CD8$^+$ (ii) T cells. Significance analysed by one-tailed unpaired Mann-Whitney test. **(B)** Flow cytometric analysis of lung parenchyma CD4$^+$ (i) and CD8$^+$ (ii) T cells from TB patients based on the expression of PD-1, CD69 and CD103 demonstrates increased PD-1 expression in the resident T cells in the lung parenchymal cells. Significance analysed by Kruskal-Wallis test with Dunn's multiple comparison test. **(C)** Immunohistochemical staining for PD-1$^+$, CD4$^+$ and CD8$^+$ expression in human lung TB granulomas. PD-1 is expressed around the central macrophage core in the same region as CD4$^+$ (ii) and CD8$^+$ (iii) T cells. Co-localization of PD-1 (blue), CD4$^+$ (red) and CD8$^+$ (yellow) using false colour of the immunostaining shows co-localisation of PD-1 with both CD4$^+$ and CD8$^+$ cells (purple and green respectively) (iv). Scale bar 100μm. **(D)** PD-1 is not expressed in caseating granulomas where immunopathology is present in human lung biopsies (i). Six biopsies taken as part of routine clinical care were studied. CD4$^+$ (ii) and CD8$^+$ (iii) expressing cells are present in the same area, and so absence of PD-1 immunoreactivity is not due to lack of viable cells. Scale bar 200μm.

Figure 2: The PD-1/ PD-L1 axis is upregulated in the 3D TB granuloma system. (A) Still images from time-lapse microscopy imaging demonstrating increasing cellular aggregation of PBMC around a focus of ultraviolet killed Mtb H37Rv in the 3D granuloma system at times 0, 12, 24 and 48h post encapsulation in the matrix. The Z projection shows the cells contained within the designated volume in a 2D reconstruction. Full time course in Video 1. **(B)** Gene expression of PD-1 and its ligands in the 3D microsphere model. RNA was extracted from live Mtb-infected PBMC and relative expression investigated by qRT-PCR at day 4 post infection. Open bars, normoxia, filled bars 1% hypoxia. PD-L1 and PD-L2 are upregulated by Mtb infection, and in 1% hypoxia PD-1 expression is increased and PD-L2 expression further augmented (n=4). Results are normalised against the housekeeping genes GAPDH, β-Microbulin and FANTA and showed similar results. β-microglobulin used for (B). *$p<0.05$, **$p<0.01$. **(C-E)** Surface expression of PD-1 and PD-L1. PBMCs were decapsulated from

741 Mtb-infected microspheres at day 7 and surface expression of PD-1 and its ligand PD-L1 were

742 analysed by flow cytometry. PD-1 is expressed in CD4^{+} (C) and CD8^{+} (D) T cells in PBMC from Mtb

743 infected microspheres incubated in normoxia. PD-1 expression was significantly upregulated in 1%

744 hypoxia. Representative flow cytometry plots and level of expression of PD-1 by the CD4^{+} and CD8^{+}

745 T cell fractions are shown (n=4). (E) PD-L1 expression on CD14^{+}CD11b^{+} cells within PBMC in Mtb

746 infected microspheres is upregulated in both normoxia and 1% hypoxia at day 7 (n=4). Significance

747 of *p<0.05. (F) Growth of Mtb H37Rv ffLux+ in microspheres in normoxia and 1% hypoxia

748 measured at day 3, 7 and 14. Hypoxia reduces Mtb growth. (G) Hypoxia inducible factor 1α (HIF-

749 1α) mRNA levels were increased in Mtb-infected microspheres incubated in 1% hypoxia. RNA was

750 extracted from decapsulated microspheres and normalised to uninfected microspheres in the same

751 environment. Results were normalised to the housekeeping genes GAPDH, β-microglobulin and

752 FANTA to check the housekeeping gene are not affected by hypoxia. Similar results all three of the

753 housekeeping genes. β-microglobulin used for this graph. Significance *** p<0.001.

754 **Figure 3: PD-1 pathway inhibition increases Mtb growth. (A)** Inhibition of PD-1 receptors by

755 small chemical inhibitor 1 increases Mtb growth in a dose-response manner (1-1000nM). Inhibitor

756 concentration 1nM (green), 10nM (purple), 100nM (blue) and 1μM (red). **(B)** Inhibitor 1 was not

757 toxic to Mtb-infected PBMC, analysed by CytoTox-Glo assay (Day 7). **(C)** Cellular toxicity was no

758 different at day 14 as analysed by LDH release. Concentration 1 and 1000nM were analysed for

759 toxicity. **(D)** Spartalizumab, a therapeutic monoclonal anti-PD-1 antibody, progressively increased

760 Mtb growth in microspheres in normoxia in a dose-dependent manner. **(E)** Spartalizumab also

761 increased Mtb growth in hypoxia. Media (black), isotype (blue), spartalizumab 20μg/ml (green) and

762 200μg/ml (red). **(F)** The anti-PD-1 antibody had no effect on cell survival in microspheres in

763 normoxia (clear bars) and 1% hypoxia (filled bars). Cytotoxicity is determined by measuring LDH

764 release at day 14 and normalized by the control. ****p<0.0001.

765 **Figure 4: PD-1 inhibition increases secretion of multiple cytokines and growth factors.** PD-1/PD-

766 L1 signalling was inhibited by Spartalizumab, a humanized IgG4 anti-PD1 monoclonal antibody, in

767 Mtb-infected microspheres at 20 and 200μ/ml in normoxia. Supernatants were collected at day 14 and

accumulation of cytokines and growth factors was analysed by Luminex 35-multiplex assay. Concentrations were normalized to secretion by Mtb infected microspheres to demonstrate relative fold change, and individual concentrations are shown in Supplementary figure 6. The experiment was performed twice with three replicates. Red font: ** $p<0.001$ for Spartalizumab versus isotype control.

Figure 5: Addition of TNF-α increases Mtb growth in microspheres in normoxia. Recombinant human G-CSF, GM-CSF, IL-4, IL-6, IL-10, IL-12, TNF-α, IL-1RA, MIP-1α, MIP-1β or RANTES were added either individually **(A** and **B)** or in combination pools **(C)** to Mtb-infected microspheres at "low" concentrations, defined as that measured in media around spheres after anti-PD-1 treatment. Recombinant human TNF-α increases growth of Mtb, whilst other pro-inflammatory cytokines did not **(A).** GM-CSF has a lesser growth-promoting effect **(B).** The only combination pool that increased Mtb growth was the pro-inflammatory cytokine pool, containing TNF-α **(C)**. **(D)** TNF-α results in a dose-dependent increase in the Mtb growth over time. **(E)** Anti-TNF-α neutralising antibodies partially suppress the increased Mtb growth caused by TNF-α augmentation. Anti-TNF-α from Thermo Fisher Scientific. **(F)** Anti-PD1 antibody incorporation within microspheres increases of Mtb growth at day 7, and this effect is reversed by concurrent anti-TNF-α neutralising antibodies within microspheres. The constituent of the cytokine pools are: Growth factor pool (GF: GM-CSF and G-CSF), Anti-Inflammatory cytokine pool (Anti-Inf: IL-10 and IL-1RA), Pro-Inflammatory cytokine pool (Pro-Inf: TNF-α, IL-6 and IL-12) and Chemokine pool (Chemo: RANTES, MIP-1α, MIP-1β).

Figure 6: TNF-α is expressed in human TB granulomas and sputum TNF-α concentrations negatively correlate with circulating PD-1 expression. (A) TNF-α is expressed within human lung TB granulomas, with greater immunoreactivity than control lung tissue at the excision margin of lung cancer (i & ii). Quantification of TNF-α immunostaining (n=5) in TB cases was significantly higher than controls (n=5) (iii). **(B)** TNF-α immunostaining was extensive in the lung granuloma of a patient that developed TB whilst treated with pembrolizumab, a humanized anti-PD-1 antibody (n=1). **(C)** CD4^{+} T cell PD-1 expression on circulating PBMC negatively correlates with sputum TNF-α concentration in a separate cohort where paired sputum and PBMCs samples are available. Green

795   dots, healthy controls; Black TB cases; Orange respiratory symptomatics. Analysis by Spearman's

796   correlation analysis gave r-value of -0.341 with p=0.0484

797

798   **Figure supplement legends**

799

800   **Figure 1–figure supplement 1:** PD-1 expression on peripheral CD4$^+$ and CD8$^+$ T-cells is

801   predominantly on CD103- and CD69-negative cells. Significance was analyzed by one-tailed

802   unpaired Mann-Whitney test.

803   **Figure 1–figure supplement 2:** PD-1 expressing cells are absent in the immediate region surrounding

804   caseous necrosis in human TB granulomas. Images from four different clinical samples are presented.

805   Scale bar 100μm.

806   **Figure 2–figure supplement 1:** Hypoxia alone has no significant effect on expression of the PD-

807   1/PDL-1/2 axis. Gene expression PD-1 and its ligands in uninfected cells was compared between

808   normoxic and hypoxic conditions in the microsphere model. RNA was extracted from uninfected

809   PBMCs and relative expression investigated by qRT-PCR at day 4. Open bars PD-1, filled bars PD-

810   L1 and black bars PD-L2 respectively. Results were normalised against the housekeeping genes

811   GAPDH, β-Microbulin and FANTA and showed similar results. No significant changes in gene

812   expression were noted in uninfected microspheres. β-microglobulin used for the analysis presented.

813   **Figure 2–figure supplement 2: (A)** Mtb H37Rv ffluc+ growth in 1% hypoxia. Microspheres were

814   decapsulated in a media containing 5mM EDTA and 0.1% saponin at day 14. The lysate was

815   centrifuged, re-suspended in 1ml PBS, serially diluted and grown in Middlebrook 7H11 media for 3

816   weeks before colony counting. **(B)** Host cell viability using 3D CytoxGlo viability assay (Promega)

817   shows no significant difference between normoxia (open bars) and hypoxia (filled bars) at day 4 and

818   day 7.

819   **Figure 3–figure supplement 1**: Small chemical inhibition of PD-1/PD-L1 interaction in 1% hypoxia

820   measured at day 14 shows a dose-dependent increase in Mtb growth with PD-1 inhibition. ***

821   $p<0.0001$ with one-way ANOVA with Dunnett's multiple comparison test.

822   **Figure 4–figure supplement 1**: Cytokine accumulation around microspheres after inhibition of PD-

823   1/PD-L1 signalling with Spartalizumab, a humanized IgG4 anti-PD1 monoclonal antibody at 20 and

824   200µg/ml in normoxia (N) and 1% hypoxia (H). Supernatants were collected at day 14 and a Luminex

825   35-multiplex assay was performed. The experiment was performed twice with three replicates.

826   Concentrations are in pg/ml. Labels in red correspond to significantly raised cytokine values. Red

827   font: Significance **$p<0.001$.

828   **Figure 4–figure supplement 2:** PD-1 inhibition increases secretion of multiple cytokines and growth

829   factors in 1% hypoxia.   Supernatants were collected at day 14 and accumulation of cytokines and

830   growth factors was analysed by Luminex 35-multiplex assay. Concentrations were normalized to

831   secretion by Mtb infected microspheres to demonstrate relative fold change, and individual

832   concentrations are shown in Supplementary figure 5. The experiment was performed twice with three

833   replicates.   Red font: ** $p<0.001$ for Spartalizumab versus Isotype control.

834   **Figure 4–figure supplement 3:** Spartalizumab induces TNF-α secretion in uninfected and infected

835   microspheres, which is neutralised by anti-TNF-α.   PBMCs which were uninfected or infected with

836   Mtb were encapsulated in alginate-collagen matrix after pre- incubation in Spartalizumab at

837   200µg/ml. The supernatant was collected to measure TNF-α secretion at day 7. (A) Spartalizumab

838   induces TNF-α secretion in uninfected cells above background, which is accentuated with Mtb

839   infection. (B) Anti-PD-1 antibody increases TNF-α secretion from Mtb infected cells above isotype,

840   and the detectable levels are suppressed by anti-TNF antibody (50µg/ml).

841   **Figure 5–figure supplement 1:** Individual Mtb growth curves at "high" cytokine concentration, five

842   times the concentration measured in media after anti-PD-1 treatment. Human recombinant G-CSF,

843   GM-CSF, IL-4, IL-6, IL-10, IL-12, TNF-α, IL-1RA, MIP-1α, MIP-1β and RANTES were added to

844   microspheres either individually or in combination pools to microspheres at 5 times the concentrations

845   in Figure 5, determined by the concentration measured in the media around the microspheres. TNF-α

846   increases Mtb growth in microspheres alone and in the pro-inflammatory pool.

847   **Figure 5–figure supplement 2:** Anti-TNF-α neutralizing antibodies supress the Mtb growth

848   following TNF-α from a different source (Anti-TNF-α from Sigma-Aldrich, UK).

849   **Figure 5–figure supplement 3:** TNF-α skews polarization of monocytes to macrophages with lower

850   CD80 expression. PBMCs were infected with Mtb H37Rv at MOI of 0.1 and encapsulated in alginate-

851   collagen microspheres after overnight incubation. Microspheres were then incubated in complete

852   RPMI (with L-Glutamine and 10% human serum) with TNF-α 7.5ng/ml. Uninfected PBMCs were

853   encapsulated and treated similarly as a comparator for TNF-α stimulation. At day 7, the microspheres

854   were decapsulated in 0.5mM EDTA solution at pH of 7.2. Double staining with CD14 and CD11b

855   defined macrophages, which were classified by CD80 and CD163 expression. (A) Histogram showing

856   expression of CD163 and CD80 where there was significant decrease in CD80 expression as shown if

857   Figure (B). TNF suppressed the relative geometric mean of CD80, but did not affect CD163

858   expression. This experiment was performed in 4 separate donors.

859   **Figure 5–figure supplement 4:** Hierarchical gating strategy used to identify lymphocyte and

860   monocytic populations from decapsulated microspheres containing human peripheral blood

861   monocular cells. Single cells were decapsulated from microspheres in 5mM EDTA, washed and

862   processed for flow cytometry. First doublets were excluded from live cells, then cells were gated as

863   CD3+ and CD3- . Subsequently, lymphocytes were further classified into CD4+ and CD8+, which are

864   sub-categorized based on PD-1 staining. Double staining with both CD14 and CD11b defined

865   macrophages, which were further analysed for PD-L1, CD80 and CD163 surface expression. All the

866   antibodies and clone number are listed in the text and the key resources table.

867

868   **Supplementary file 1:** PD-1 expressing cells for each subset expressed as percentage of live CD45+

869   cells, with range in parentheses.

870

871   **Video 1:** Cell migration over 48 hours around a central cluster of

872   macrophages infected with UV-killed Mtb within a 3D alginate-collagen matrix. Migration is seen in

873   the first 24 hours, without aggregation, and then progressive granuloma formation occurs.

874

875

(A)

i

p = 0.0622

Frequency of PD-1+CD4+ Cells

Blood   Lung

ii

p = 0.0240

Frequency of PD-1+CD8+ Cells

Blood   Lung

(B)

i

p = 0.0002

p = 0.0002

p = 0.0005

Frequency of CD4+PD-1+

CD103+CD69-   CD103+CD69+   CD103-CD69+   CD103-CD69-

ii

p = 0.0007

p = 0.0005

p = 0.0034

Frequency of CD8+ PD-1+

CD103+CD69-   CD103+CD69+   CD103-CD69+   CD103-CD69-

(C)

i   ii   iii   iv

(D)

i   ii   iii

(A) 0h, 12h, 24h, 48h; scale bars 65μm

(B) RNA Fold Change (Log 2) vs Control, PD-1, PD-L1, PD-L2

(C) i: PD-1 on CD3+CD4+ T cells (Mtb-Hypoxia, Mtb-Normoxia, Media); ii: Change in MFI (Media, Normoxia, Hypoxia) Mtb

(D) i: PD-1 on CD3+CD8+ T cells (Mtb-Hypoxia, Mtb-Normoxia, Media); ii: Change in MFI (Media, Normoxia, Hypoxia) Mtb

(E) i: PD-L1 on CD14+CD11b+ cells (Mtb-Hypoxia, Mtb-Normoxia, Media); ii: Change in MFI (Media, Normoxia, Hypoxia) Mtb

(F) Bacterial Growth (Log RLU) vs Day; Mtb-Normoxia, Mtb-Hypoxia

(G) RNA Fold Change (Log2); Normoxia, Hypoxia

(A)

Mtb growth (RLU)

***

Day

- Mtb
- TNF-α
- IL-12
- IL-6
- IL-10
- IL-1RA

(B)

Mtb growth (RLU)

**

Day

- Mtb
- MIP-1β
- MIP-1α
- RANTES
- G-CSF
- GM-CSF

(C)

Mtb growth (RLU)

***

Day

- Mtb
- GF
- Anti-Inf
- Pro-Inf
- Chemo

(D)

Mtb growth (RLU)

Day

- Mtb
- 15
- 1.5
- 0.15
- 0.015

(E)

Mtb growth (RLU)

Mtb	+	+	+	+	+	+	+	+	+	+
TNF-α (ng/ml)	-	-	15	15	1.5	1.5	0.15	0.15	0.015	0.015
Anti-TNF-α(50 µg/ml)	-	+	-	+	-	+	-	+	-	+

(F)

Mtb growth (RLU)

* *

Mtb	+	+	+	+
Ab-PD1(200µg/ml)	-	+	-	+
Ab-TNF-α (50µg/ml)	-	-	+	+

(A)

i

ii

iii

Lung cancer

TB

TNF-α Staining (Density/Cell)

$2×10^8$
$1.5×10^8$
$1×10^8$
$5×10^7$
0

****

Control   TB Cases

(B)

(C)

r= -0.341   p= 0.0484

Sputum TNF-a (pg/mg Total P rotein)

1000
100
10
1

0   25   50   75   100

CD4+ PD1+ (%)

Figure 1–figure supplement 1: PD-1 expression on peripheral CD4$^+$ and CD8$^+$ T-cells is predominantly on CD103- and CD69-negative cells. Significance was analyzed by one-tailed unpaired Mann-Whitney test.
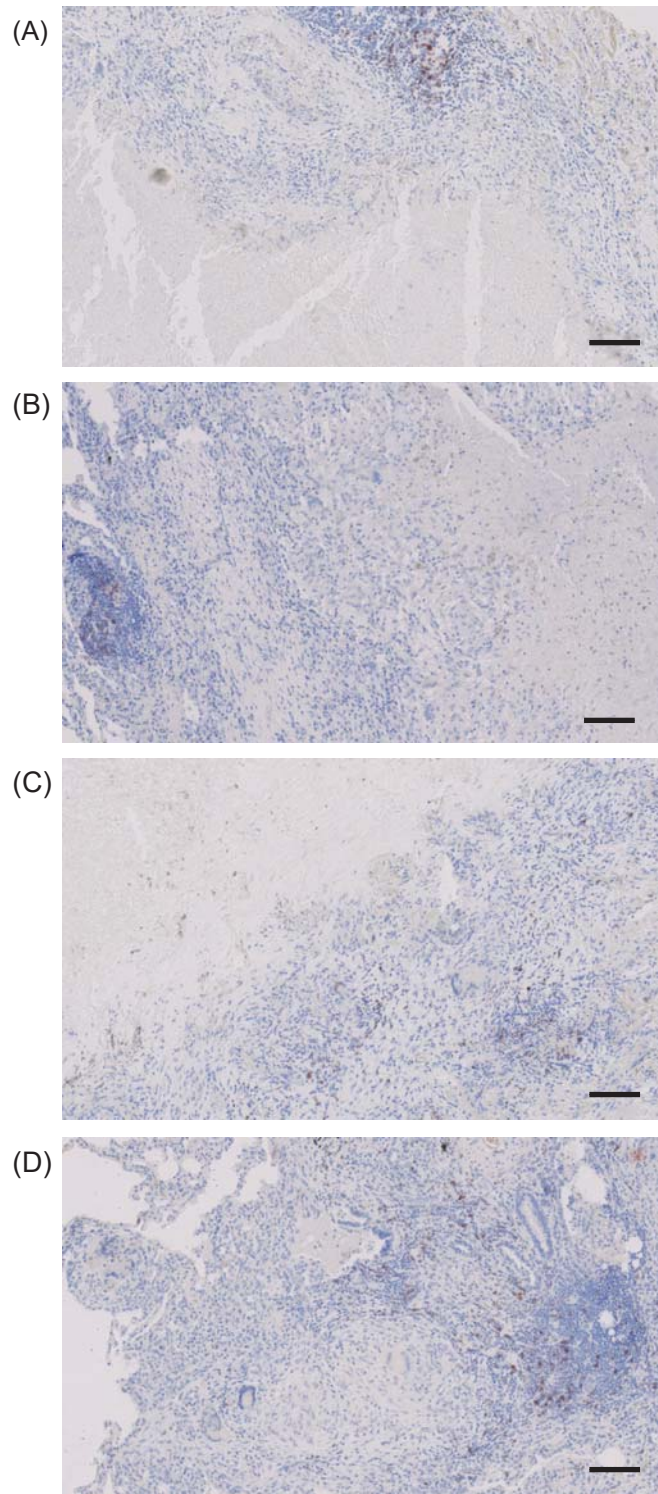
Figure 1–figure supplement 2: PD-1 expressing cells are absent in the immediate region surrounding caseous necrosis in human TB granulomas. Images from four different clinical samples are presented. Scale bar 100μm.
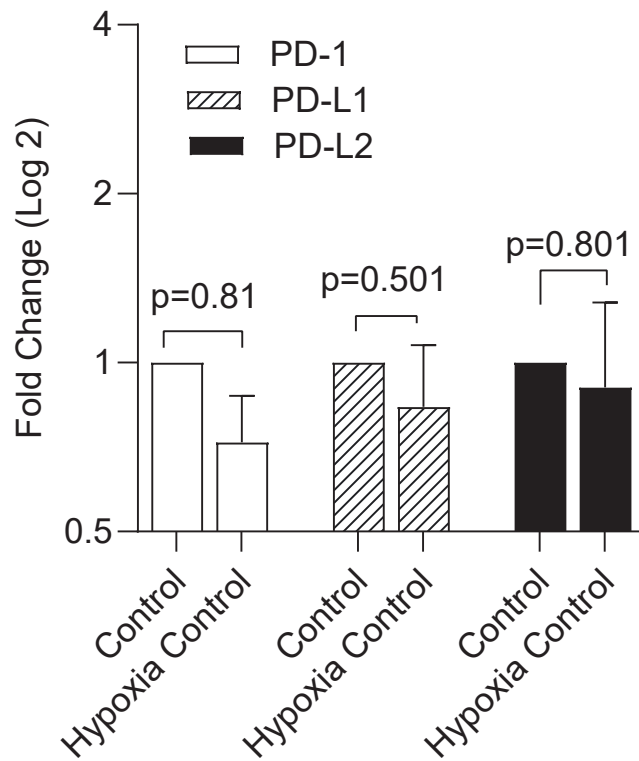
Figure 2–figure supplement 1: Hypoxia alone has no significant effect on expression of the PD-1/PDL-1/2 axis. Gene expression PD-1 and its ligands in uninfected cells was compared between normoxic and hypoxic conditions in the microsphere model. RNA was extracted from uninfected PBMCs and relative expression investigated by qRT-PCR at day 4. Open bars PD-1, filled bars PD-L1 and black bars PD-L2 respectively. Results were normalised against the housekeeping genes GAPDH, β-Microbulin and FANTA and showed similar results. No significant changes in gene expression were noted in uninfected microspheres. β-microglobulin used for the analysis presented.
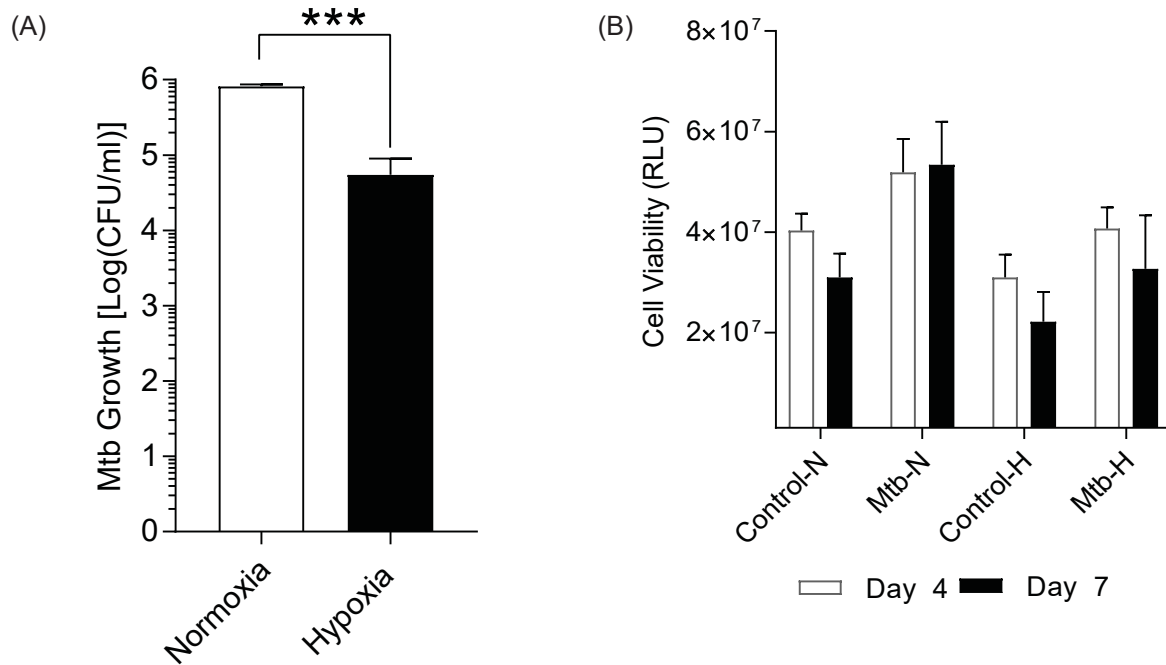
Figure 2–figure supplement 2A: **(A)** Mtb H37Rv ffluc+ growth in 1% hypoxia. Microspheres were decapsulated in a media containing 5mM EDTA and 0.1% saponin at day 14. The lysate was centrifuged, re-suspended in 1ml PBS, serially diluted and grown in Middlebrook 7H11 media for 3 weeks before colony counting. **(B)** Host cell viability using 3D CytoxGlo viability assay (Promega) shows no significant difference between normoxia (open bars) and hypoxia (filled bars) at day 4 and day 7.
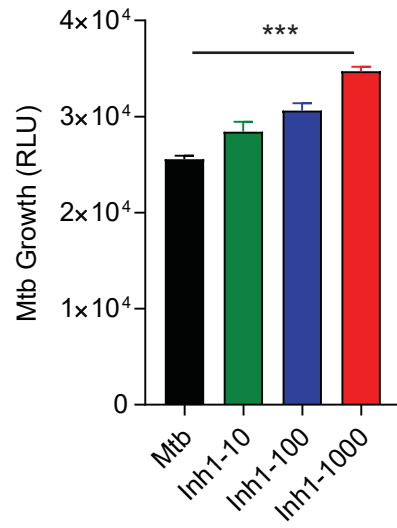
Figure 3–figure supplement 1: Small chemical inhibition of PD-1/PD-L1 interaction in 1% hypoxia measured at day 14 shows a dose-dependent increase in Mtb growth with PD-1 inhibition. *** $p < 0.0001$ with one-way ANOVA with Dunnett's multiple comparison test.
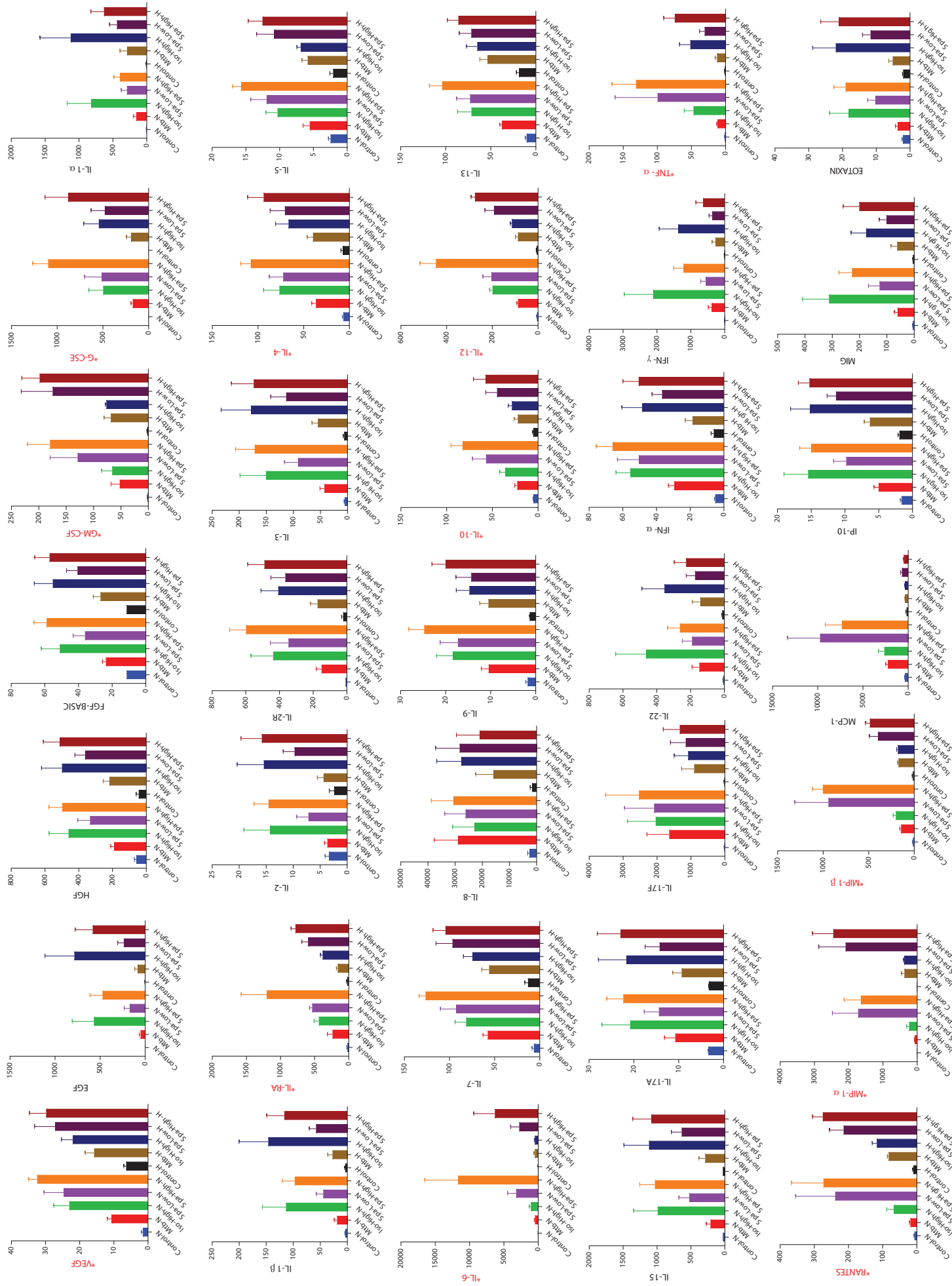
Figure 4-figure supplement 1 (*legend overleaf*)

Figure 4–figure supplement 1: Cytokine accumulation around microspheres after inhibition of PD-1/PD-L1 signalling with Spartalizumab, a humanized IgG4 anti-PD1 monoclonal antibody at 20 and 200μg/ml in normoxia (N) and 1% hypoxia (H). Supernatants were collected at day 14 and a Luminex 35-multiplex assay was performed. The experiment was performed twice with three replicates. Concentrations are in pg/ml. Labels in red correspond to significantly raised cytokine values. Red font: Significance **p<0.001.
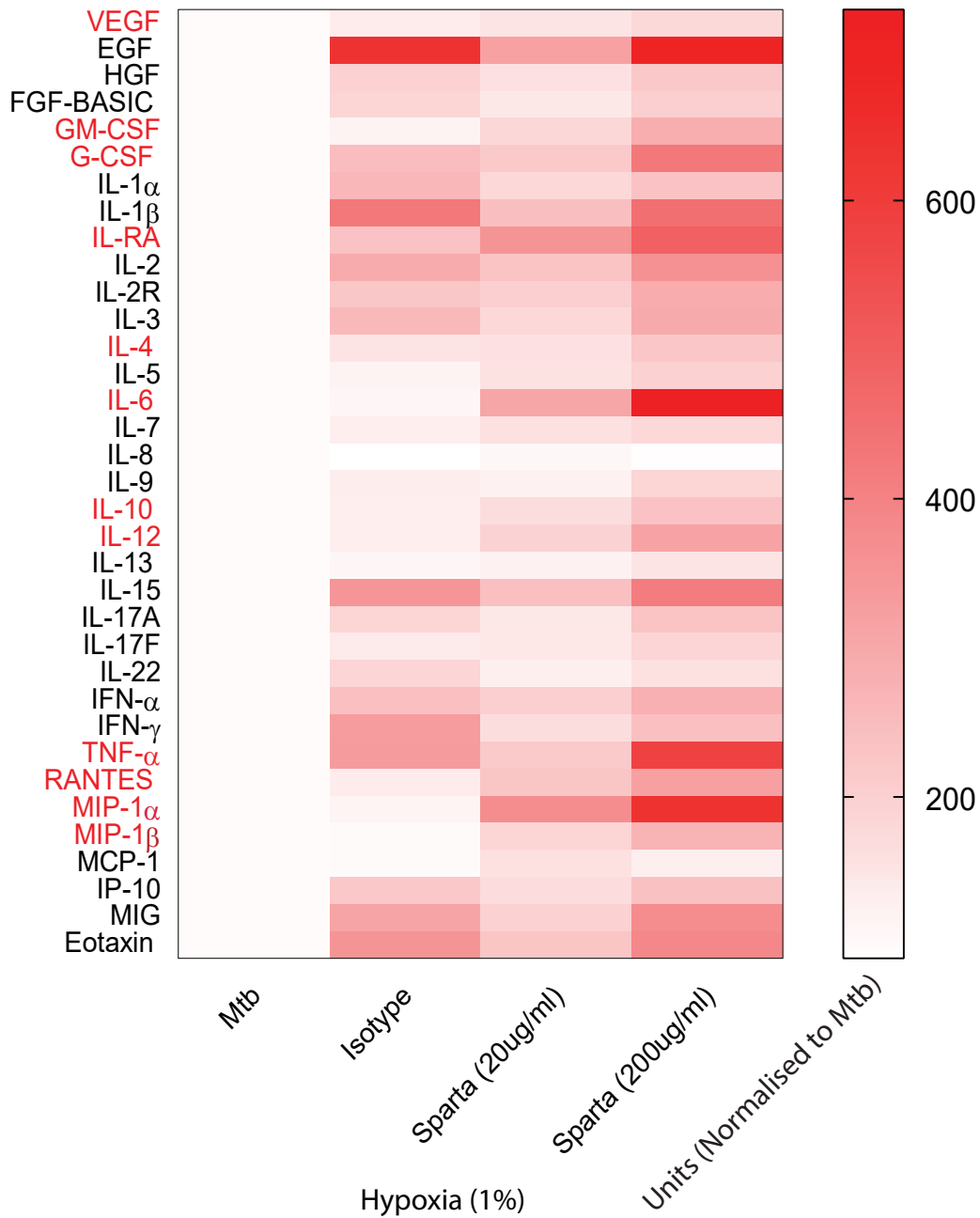
Figure 4–figure supplement 2: PD-1 inhibition increases secretion of multiple cytokines and growth factors in 1% hypoxia. Supernatants were collected at day 14 and accumulation of cytokines and growth factors was analysed by Luminex 35-multiplex assay. Concentrations were normalized to secretion by Mtb infected microspheres to demonstrate relative fold change, and individual concentrations are shown in Supplementary figure 5. The experiment was performed twice with three replicates. Red font: ** $p<0.001$ for Spartalizumab versus Isotype control.

Figure 4–figure supplement 3: Spartalizumab induces TNF-α secretion in uninfected and infected microspheres, which is neutralised by anti-TNF-α. PBMCs which were uninfected or infected with Mtb were encapsulated in alginate-collagen matrix after pre- incubation in Spartalizumab at 200μg/ml. The supernatant was collected to measure TNF-α secretion at day 7. (A) Spartalizumab induces TNF-α secretion in uninfected cells above background, which is accentuated with Mtb infection. (B) Anti-PD-1 antibody increases TNF-α secretion from Mtb infected cells above isotype, and the detectable levels are suppressed by anti-TNF antibody (50μg/ml).
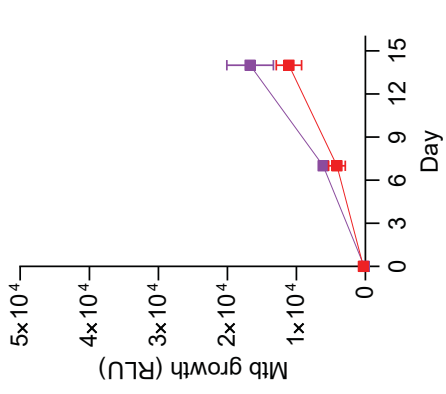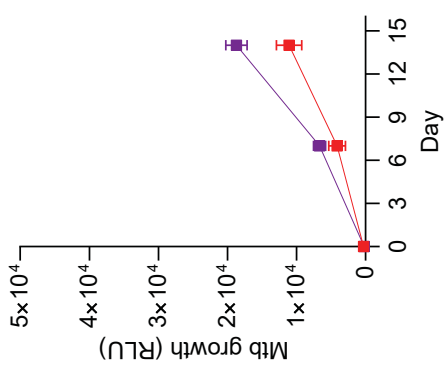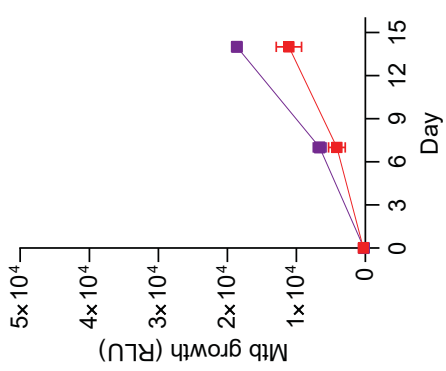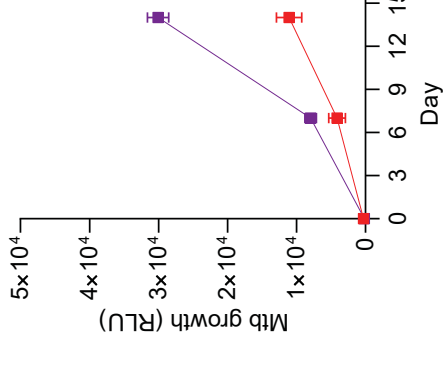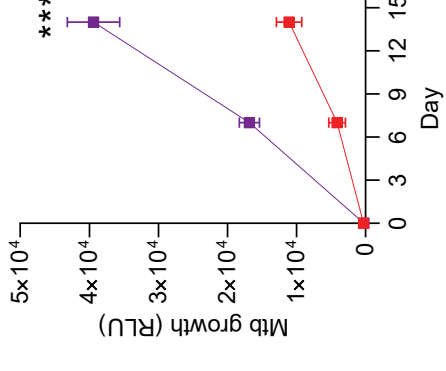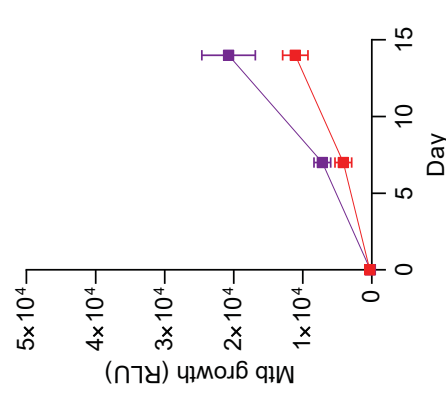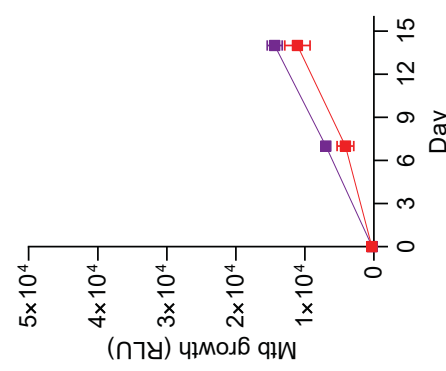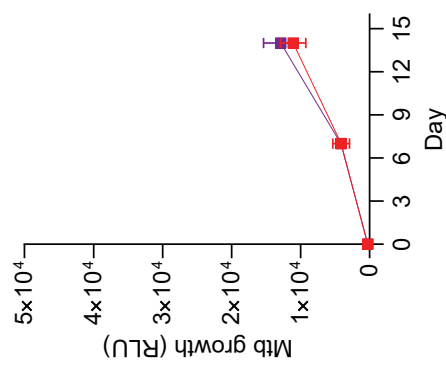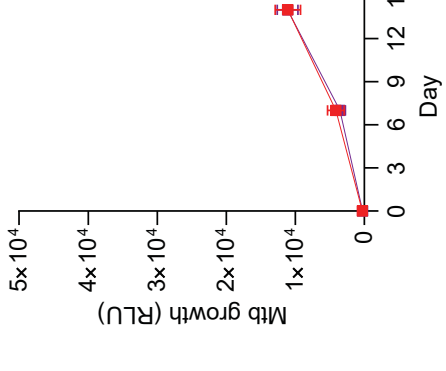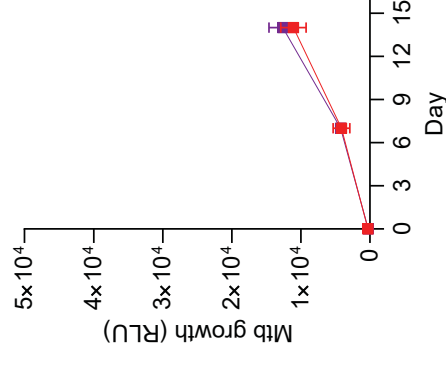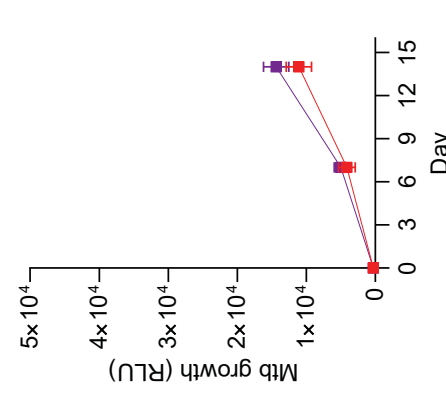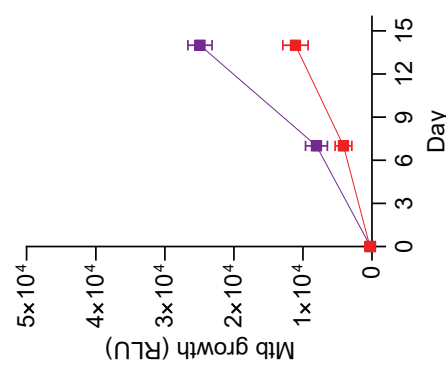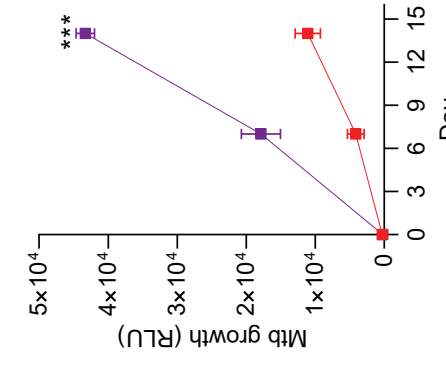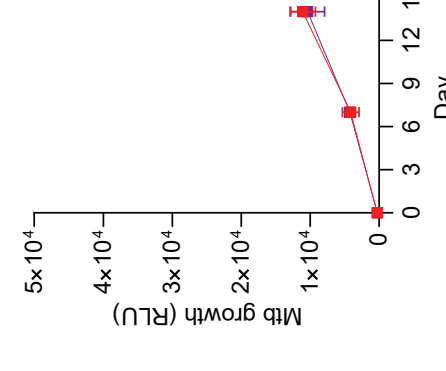
Figure 5–figure supplement 1: Individual Mtb growth curves at "high" cytokine concentration, five times the concentration measured in media after anti-PD-1 treatment. Human recombinant G-CSF, GM-CSF, IL-4, IL-6, IL-10, IL-12, TNF-α, IL-1RA, MIP-1α, MIP-1β and RANTES were added to microspheres either individually or in combination pools to microspheres at 5 times the concentrations in Figure 5, determined by the concentration measured in the media around the microspheres. TNF-α increases Mtb growth in microspheres alone and in the pro-inflammatory pool.
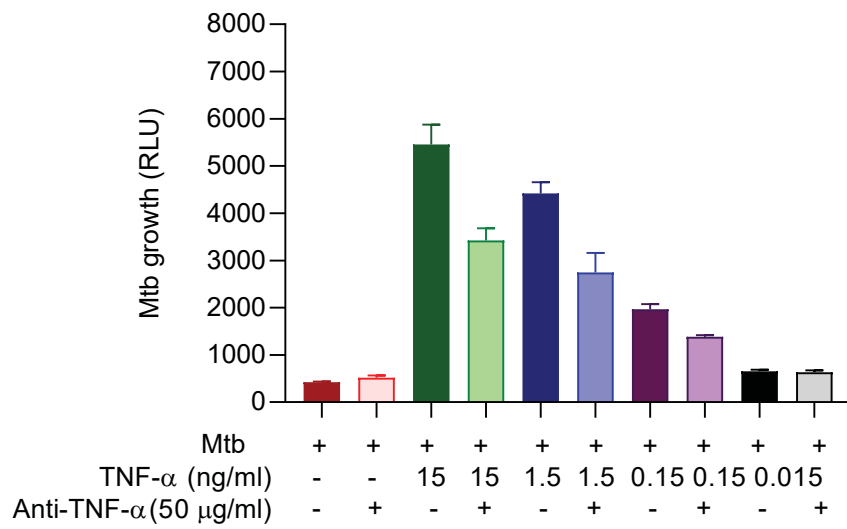
Figure 5–figure supplement 2: Anti-TNF-α neutralizing antibodies supress the Mtb growth following TNF-α from a different source (Anti-TNF-α from Sigma-Aldrich, UK).
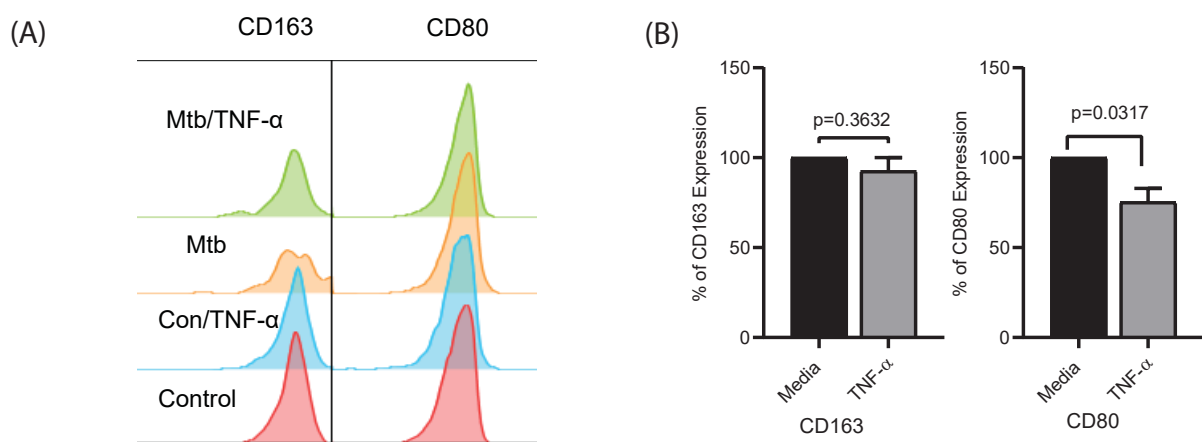
Figure 5–figure supplement 3: TNF-α skews polarization of monocytes to macrophages with lower CD80 expression. PBMCs were infected with Mtb H37Rv at MOI of 0.1 and encapsulated in alginate-collagen microspheres after overnight incubation. Microspheres were then incubated in complete RPMI (with L-Glutamine and 10% human serum) with TNF-α 7.5ng/ml. Uninfected PBMCs were encapsulated and treated similarly as a comparator for TNF-α stimulation. At day 7, the microspheres were decapsulated in 0.5mM EDTA solution at pH of 7.2. Double staining with CD14 and CD11b defined macrophages, which were classified by CD80 and CD163 expression. (A) Histogram showing expression of CD163 and CD80 where there was significant decrease in CD80 expression as shown if Figure (B). TNF suppressed the relative geometric mean of CD80, but did not affect CD163 expression. This experiment was performed in 4 separate donors.
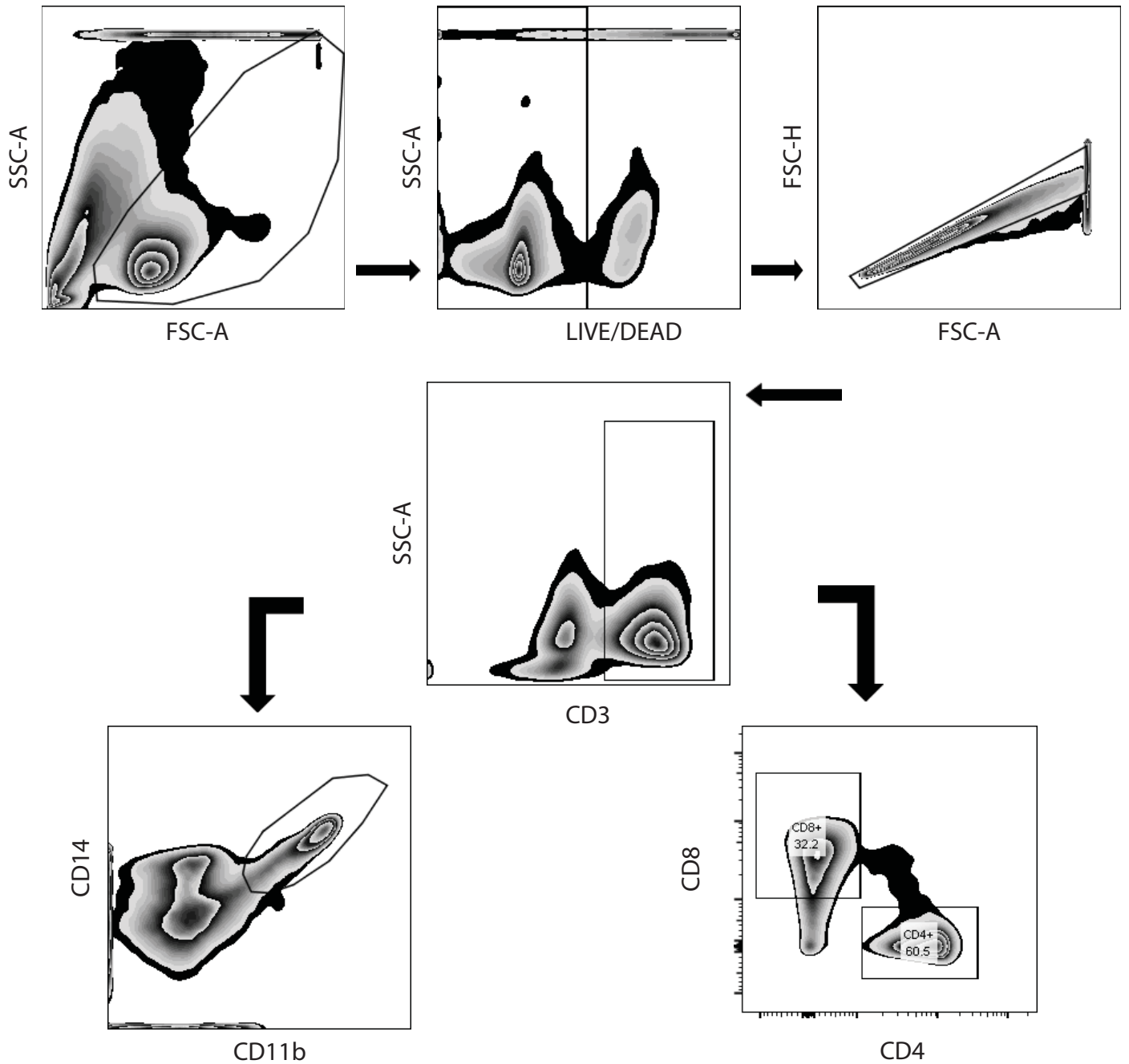
Figure 5–figure supplement 4: Hierarchical gating strategy used to identify lymphocyte and monocytic populations from decapsulated microspheres containing human peripheral blood monocular cells. Single cells were decapsulated from microspheres in 5mM EDTA, washed and processed for flow cytometry. First doublets were excluded from live cells, then cells were gated as CD3+ and CD3- . Subsequently, lymphocytes were further classified into CD4+ and CD8+, which are sub-categorized based on PD-1 staining. Double staining with both CD14 and CD11b defined macrophages, which were further analysed for PD-L1, CD80 and CD163 surface expression. All the antibodies and clone number are listed in the text and the key resources table.